

**Best Available
Copy
for all Pictures**

AD-768 907

HIGH PERFORMANCE HOLLOW PROJECTILES

Scott Rethorst, et al

Vehicle Research Corporation

Prepared for:

Advanced Research Projects Agency

17 August 1973

DISTRIBUTED BY:

NTIS

National Technical Information Service
U. S. DEPARTMENT OF COMMERCE
5285 Port Royal Road, Springfield Va. 22151

4D 768 907

HIGH PERFORMANCE HOLLOW PROJECTILES

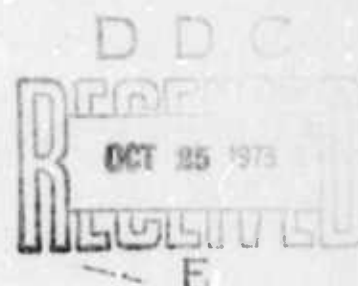
by

Scott Rethorst, Toshio Fujita,
J. J. Wu, E. R. Sargent, Robert Berlot

Sponsored by
Advanced Research Projects Agency

ARPA Order No. 1575
Amendment No. 6, dated 10/18/71

FINAL TECHNICAL REPORT
Small Arms Systems Agency
Contract No. DAAD05-72-C-0296



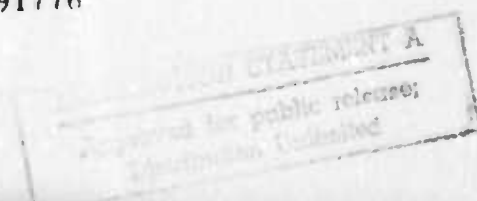
VRC Report No. 26

17 August 1973

The views and conclusions contained in this document are those of the authors and should not be interpreted as necessarily representing the official policies, either expressed or implied, of the Advanced Research Projects Agency or the U.S. Government

Reproduced by
NATIONAL TECHNICAL
INFORMATION SERVICE
U S Department of Commerce
Springfield VA 22151

VEHICLE RESEARCH CORPORATION
418 South Pine Street
San Gabriel, California 91776
(213) 287-9781



ACKNOWLEDGMENT

This research was sponsored by the Advanced Research Projects Agency of the Department of Defense and was monitored by the U.S. Small Arms Systems Agency under Contract No. DAAD05-72-C-0296.

The authors wish to express their appreciation to Mr. George Fussell of ARPA for his support and overall direction. The authors also gratefully acknowledge the detailed assistance and guidance of Mr. Carl Bysura of SASA and the general support and encouragement provided by Mr. Leo Ambrosini, Dr. Dave Katsanis, Colonel Iserson, and the staff of SASA. The effort of Mrs. Alrae Tingley in typing and publication of this report is also greatly appreciated.

FOREWORD

Development of hollow projectiles was first advocated by VRC (letter proposal of 1969) to achieve "silent" (low pressure signal) projectiles having higher performance. In response to a Government review a more detailed and expanded proposal (VRC Proposal No. P-748) was submitted in 1970 and this ultimately led to the present ARPA/SASA effort which focuses on demonstration of high performance characteristics.

Although the present VRC effort concentrates on small arms (specifically 7.62 mm), the confirmed fundamental theory applies to all sizes of hollow projectiles. This report can thus serve as a basis for (1) evaluating specific hollow projectile developments and (2) formulating programs to develop a wide spectrum of hollow projectile configurations tailored to a diversity of functional requirements.

SUMMARY

Hollow projectiles are shown to have potential for providing an order of magnitude improvement over conventional small arms ammunition. They provide high performance (high energy delivery at high speed) and vastly improved operational characteristics at a low cost. This was theoretically established and experimentally demonstrated via both wind tunnel and firing range tests.

Hollow projectiles achieve much lower drag by essentially eliminating both wave and base drag. This directly increases energy delivery and speed. The hollow configuration further permits compact lightweight designs having high speeds with improved impact/penetration characteristics. The projectiles are basically thin-walled hollow tubes with beveled ends and are therefore very inexpensive.

The basic hollow projectile characteristics of low drag over a wide operating range were first theoretically established. Then, these characteristics were confirmed via wind tunnel tests involving Schlieren photography and force measurements. Firing range tests then showed that hollow projectiles can be (1) sabot-launched at high speeds, (2) spin stabilized for reasonable accuracy and dispersion characteristics with potential for large improvement and (3) applied to missions requiring improved armor penetration characteristics.

The present effort has thus established a basic theoretical and experimental foundation which is broadly applicable to the entire size spectrum of hollow projectile ammunition. For initial demonstration purposes, simple base "plug" sabots were employed to fire 7.62 mm projectiles. Exploratory investigations of compact arrangements (e.g., puller sabots allowing propellant to be packaged inside the hollow projectile) suitable for practical small arms ammunition yielded promising results regarding further development.

Additionally, simple and inexpensive methods of imparting spin for stabilization were developed. The projectiles were coated with a thin outer layer of soft metals (e.g., copper) and soft plastics (e.g. polypropylene) which engaged the rifling. This greatly simplifies sabot design and will significantly contribute to the ultimate goal of developing practical ammunition systems. The coating development was conducted to the point of demonstrating basic feasibility.

Further feasibility demonstration work is recommended to ascertain or quantify the extent to which the high potential can be achieved in practical compact ammunition systems. This will entail a carefully focused study involving the interaction of aerodynamic/ballistic performance and design features providing compact, rugged and low cost ammunition.

CONTENTS

<u>Chapter</u>	<u>Title</u>	<u>Page</u>
I	INTRODUCTION	1
II	DISCUSSION	3
	A. PERFORMANCE IMPROVEMENT	3
	1. Low Drag	4
	a. Analytical Prediction	4
	b. Experimental Confirmation	9
	2. Wide Operating Range	9
	a. High Performance Region	11
	(1) Theoretical Basis	11
	(2) Test Verification	15
	b. Stable Flight Characteristics	19
	(1) Basic Stability Criteria	21
	(2) Aerodynamic Considerations	26
	(3) Firing Range Test Results	31
	3. High Penetration Capability	36
	a. Kinetic Energy Delivery	36
	b. Impact/Penetration Analysis	39
	c. Penetration Testing	43
	B. OPERATIONAL ADVANTAGES	47
	1. Compactness/Sabot Development	49
	a. Developmental Results	49
	b. Projected Systems	54
	(1) Internal Forward Sabot	54
	(2) External Forward Sabot	56
	(3) Consumable Sabot	57

<u>Chapter</u>	<u>Title</u>	<u>Page</u>
	2. Lightweight Ammunition System	57
	3. Inexpensive Manufacture/Design Simplicity . .	58
III	CONCLUSIONS AND RECOMMENDATIONS	61
IV	REFERENCES	63
	APPENDIX: EXPERIMENTAL FACILITIES AND TEST PROCEDURES	A-1
	A. SUPERSONIC WIND TUNNEL	A-1
	1. Facility Description	A-1
	2. Test Procedures	A-1
	B. MOBILE FIRING RANGE TEST SETUP . . .	A-6
	1. Facility Description	A-6
	2. Test Procedures	A-8
	APPENDIX REFERENCES	A-11

LIST OF ILLUSTRATIONS

<u>Fig. No.</u>	<u>Title</u>	<u>Page</u>
1	Fundamental Flowfield Improvement	2
2	Comparative Drag, Hollow vs. Conventional Solid Projectiles	6
3	Basic Trajectory Characteristics, Comparison of Hollow and Conventional Projectiles	8
4	Effect of Length and Speed on Drag Coefficient, 7.62 mm Hollow Projectiles	10
5	Hollow Projectile Operating Region	16
6	Determination of High Performance Region, Schlieren Photographs of HPP-1 at Zero Yaw	18
7	Hollow Projectile Range, Velocity Decay Characteristics in High Performance Region	20
8	Stability Boundaries of Spin Stabilized Hollow Projectile.	25
9	Effect of Yaw on High Performance Region, Test Model HF P-1	27
10	Experimental Lift Curve Slope	30
11	Accuracy and Dispersion Test Results, Projectile P-93; Target: 555'	33
12	Accuracy and Dispersion Test Results, Projectile P-96; Target: 555'	34
13	Accuracy and Dispersion Test Results, Projectile P-97; Target: 555'	35
14	Energy Decay Characteristics, Comparison of Hollow and Standard Projectiles	37
15	Correlation of Projectile Penetration Data and Theories.	42
16	Improved Penetration, Hollow vs. Solid Cylindrical Projectile (Equal Impact Energy)	44
17	Helmet Penetration Tests	46

<u>Fig. No.</u>	<u>Title</u>	<u>Page</u>
18	Example High Performance Compact Hollow Projectile System for 7.62 mm Weapons	48
19	Experimentally Investigated Sabot Configurations . .	50
20	Cup Sabot Separation Photographs	51
21	Plug Sabot Separation Photographs.	53
22	Projected Compact Hollow Projectile Systems . . .	55
A-1	Wind Tunnel Test Arrangement	A-2
A-2	Firing Test Setup	A-7

NOMENCLATURE

- A = projectile frontal area ($\frac{\pi}{4} d^2$)
- A_c = upstream capture area
- A_i = inlet area
- A_t = throat area
- C_D = drag coefficient
- C_L = lift coefficient
- C_l = slope of lift coefficient ($\partial C_L / \partial \delta$)
- C_M = overturning moment coefficient
- C_m = slope of overturning moment coefficient ($\partial C_M / \partial \delta$)
- C_q = damping moment coefficient
- C_t = acoustic velocity of target material
- D = drag
- d = maximum projectile diameter
- d_t = throat diameter
- E = projectile kinetic energy
- I_a = mass moment of inertia about the longitudinal axis
- I_b = mass moment of inertia about the transverse axis through the c. g.
- K = base drag coefficient
- L = lift force (normal to flight direction)
- l = projectile length
- M = Mach number
- M_s = Mach number downstream of detached shock
- M_t = Mach number in throat
- m = mass

- N = spin rate about longitudinal axis
- P = penetration depth (semi-infinite medium)
- p = ambient air pressure
- q = dynamic pressure
- r = recovery factor; projectile radius
- t = projectile wall thickness
- V = velocity
-
- β = internal bevel angle
- γ = ratio of specific heats
- δ = yaw angle of projectile measured from relative wind direction
- ϵ = nose cone half-angle (conventional projectile)
- ρ = air density
- ρ_p = density of projectile
- ρ_t = density of target
- μ = Mach wave angle

I. INTRODUCTION

This report on hollow projectiles covers work from the conception of the advantages of the projectile, through theoretical predictions of its performance, to firing tests (7.62 mm) which confirmed the theoretical predictions and demonstrated the potential superiority of this type of ammunition.

Hollow projectiles are basically thin-walled tubes with beveled ends (Fig. 1). Nearly all the air approaching the forward face of the tube flows inside the tubular projectile. The flow outside the tube remains essentially parallel and undisturbed.

Conventional projectiles, having a pointed nose and blunt base, experience a bow shock wave at the nose and a separated flow region at the base. This results in high energy dissipation and drag. Hollow projectiles substantially avoid these losses to gain an order of magnitude improvement.

The well-known desirable performance characteristics of ammunition systems are,

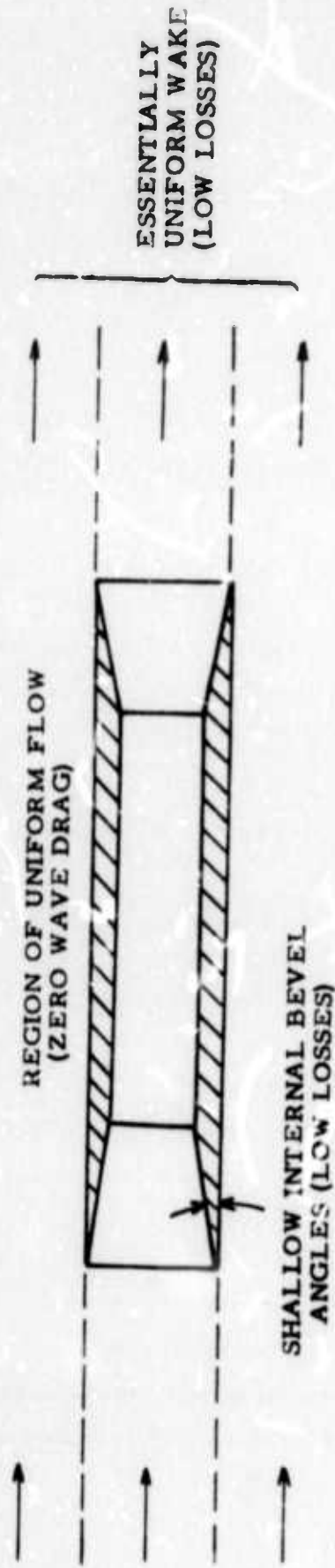
- High Speed and Impact Energy
- High Effective Range and Flat Trajectory
- Superior Target Penetration
- High Accuracy and Low Dispersion

In addition to providing improved performance, basic operational features will ultimately establish feasibility, i.e., desirable ammunition systems must have

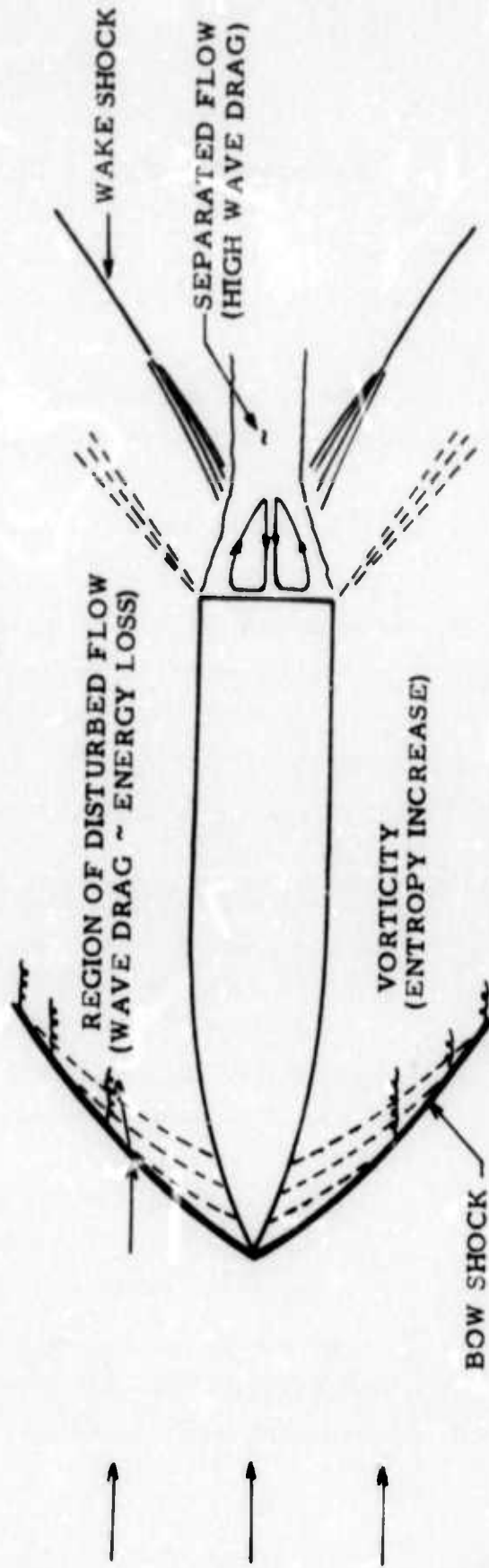
- Simplicity for Inexpensive Manufacturing
- Low Unit Weight and Compactness
- Low Recoil

Analytical/design and experimental results presented in this report demonstrate that hollow projectile ammunition systems possess the desired performance and operational characteristics listed above.

HIGH PERFORMANCE HOLLOW PROJECTILE



CONVENTIONAL PROJECTILE



FUNDAMENTAL FLOW FIELD IMPROVEMENT

Fig. 1

II. DISCUSSION

Effort was concentrated specifically on demonstrating high performance characteristics of hollow projectiles. Specific accomplishments include

- Aerodynamic/ballistic analyses to (1) determine the potential for high performance over a wide operating range and (2) establish a basis for parametric design trade-off studies directed toward compact lightweight ammunition systems.
- Wind tunnel tests to (1) confirm the basic theory by affirming the predicted character of the flow field (Schlieren visualization) and (2) demonstrate achievement of low drag.
- Firing tests to demonstrate (1) spin-stabilized launchings from standard small arms weapons (7.62 mm) at high speeds (4000 to 6000 fps) and (2) capability for high accuracy and low dispersion with superior impact/penetration in armor (P.0) nets).

A. PERFORMANCE IMPROVEMENT

The fundamental key factor leading to performance improvement is the achievement of low drag over a wide operating flight speed range. This will enable lightweight projectiles to deliver high energy to distant targets at high speeds. Higher speeds result in flatter trajectories and shorter flight times, thereby enhancing accuracy and effectiveness. Further, both higher energies and speeds are dominant factors in improving impact/penetration capabilities at the target.

1. Low Drag

The basic low drag characteristics of hollow projectiles were analytically established in Ref. 1 and presented as part of the proposal which resulted in the present program. These low drag characteristics were experimentally confirmed during the course of this program.

a. Analytical Prediction

In Ref. 1 it is shown that a conventional projectile (Fig. 1) has three basic drag sources: (1) wave drag, (2) base drag, and (3) skin friction drag. Representing a standard projectile as a cone-cylinder, the drag coefficient can be estimated by the following relation,

$$\begin{aligned} C_{Dc} = & \left[2.1 \sin^2 \epsilon + \frac{0.5 \sin \epsilon}{\sqrt{M^2 - 1}} \right] \sim \text{Wave drag} \\ & + \left[\frac{K}{\frac{1}{2} \gamma M^2} \right] \sim \text{Base drag} \\ & + \left[\frac{4l_c}{d} \left(\frac{0.074}{5\sqrt{R_{l_c}}} - \frac{1700}{R_{l_c}} \right) / \left(1 + r \frac{\gamma - 1}{2} M^2 \right) \right] \sim \text{Friction drag} \end{aligned} \quad (1)$$

The drag coefficient is based on the maximum cross sectional area of the projectile, i.e.,

$$C_{Dc} \equiv \frac{D}{\left(\frac{1}{2} \gamma M^2 p \right) A} = \frac{D}{\left(\frac{1}{2} \gamma M^2 p \right) \left(\frac{\pi}{4} d^2 \right)} \quad (2)$$

where

D = drag

M = Mach number

d = maximum projectile diameter

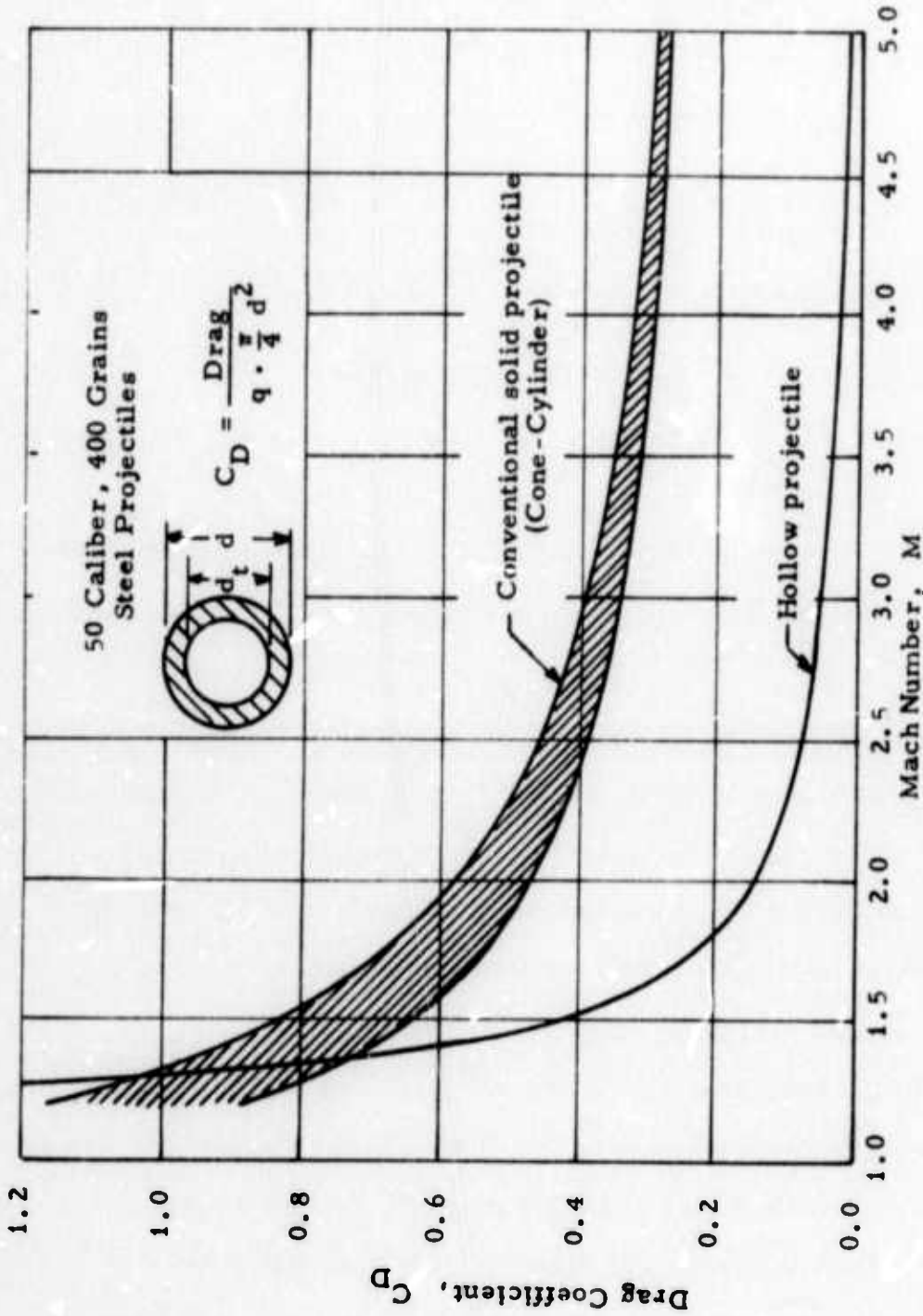
- γ = ratio of specific heats ($\gamma = 1.4$ for air)
- p = ambient air pressure
- R_{l_c} = Reynolds number based on l_c
- l_c = conventional projectile length
- K = base drag coefficient
- r = recovery factor
- ϵ = nose cone half-angle

The drag coefficient of a thin-walled hollow projectile, C_D , is basically twice the friction drag term of Eq. (1) with l_c replaced by the length of the hollow projectile denoted by l . The term is doubled since the wetted area of the hollow projectile is approximately doubled. However, the large wave and base drag terms [(Eq. (1))] are essentially eliminated.

A drag comparison of conventional and hollow projectiles is presented in Fig. 2 as a function of flight Mach number. For illustrative purposes, the comparison is based on 50-caliber steel projectiles weighing 400 grains. In the speed range of interest (i.e., $M > 2$), a large order of magnitude drag reduction is indicated.

The shaded region for the conventional projectile in Fig. 2 corresponds to the base drag coefficient range of $0.4 \leq K \leq 0.7$. Further, the recovery factor is taken to be $r = 0.85$ (Refs. 2 and 3) and the nose-half-angle is $\epsilon \approx 18.3^\circ$ while the length is $l_c \approx 1.54$ inches.

For hollow projectiles of Fig. 2 the internal diameter r was chosen to correspond to sonic flow inside the projectile. Further, if the hollow projectile is to have the same mass, it must be longer. For example, for $M \approx 3$ the hollow projectile is approximately 50%



COMPARATIVE DRAG
Hollow vs. Conventional Solid Projectiles
Fig. 2

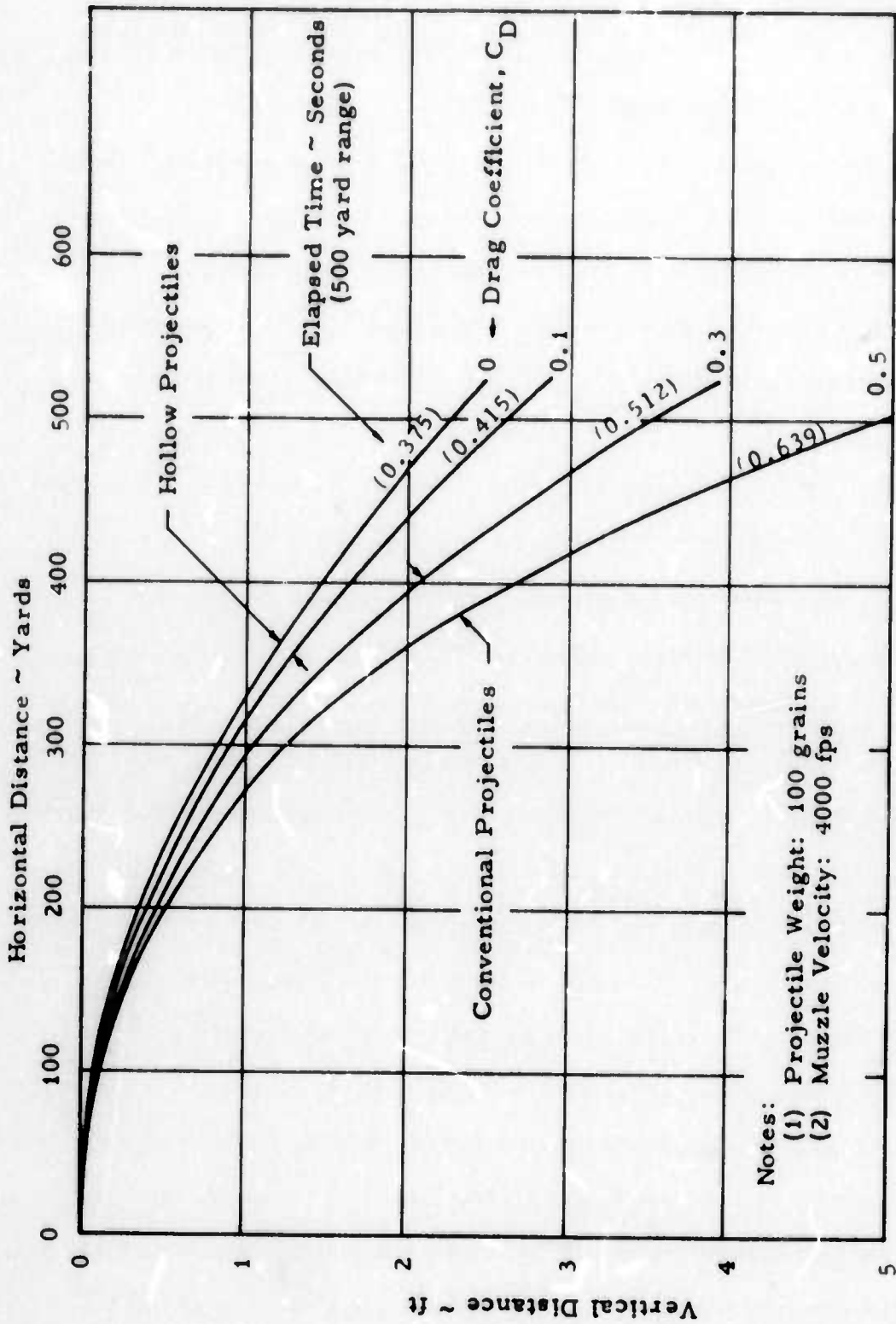
longer. The added friction drag is small compared to the savings associated with virtual elimination of wave and base drag as evident from Fig. 2.

To fully exploit the characteristics of the hollow projectile, departures will be made from the equal weight, flight speed, and sonic throat basis of comparison in Fig. 2. Generally, hollow projectiles will be lighter and faster. The throat velocity will be greater than sonic due to "starting" and operating velocity decay requirements as discussed in the next section.

The design operating conditions of a hollow projectile will actually be selected in the context of the overall weapon system and its intended application. Relevant factors include cartridge propellant volume, target range, and penetration requirements. Thus, there is no single comparison basis. However the comparison basis of Fig. 2 is certainly sufficient to clearly show the large potential for gain via drag reduction.

The reduction in drag coefficient of Fig. 2 directly improves basic projectile flight trajectory characteristics. Using well-known relationships it is shown in Fig. 3 that hollow projectiles will have roughly half the vertical displacement and elapsed time for a 500 yard range. The comparison basis of Fig. 3 is equal weight (100 grains) and muzzle velocity (4000 fps).

Since lighter hollow projectiles will generally be fired at higher muzzle velocities than conventional projectiles, the reduction in vertical displacement and elapsed time will be even greater than shown on Fig. 3. These improvements will directly improve the effectiveness of the weapon, particularly against moving targets.



BASIC TRAJECTORY CHARACTERISTICS
Comparison of Hollow and Conventional Projectiles

Fig. 3

For purposes of experimental investigation, standard 7.62 mm test equipment was utilized. Therefore, effort was concentrated on 7.62 mm hollow projectiles that could be test fired with the existing equipment. Analytically predicted drag coefficients of 7.62 mm hollow projectiles are presented in Fig. 4 as a function of projectile length and flight Mach number.

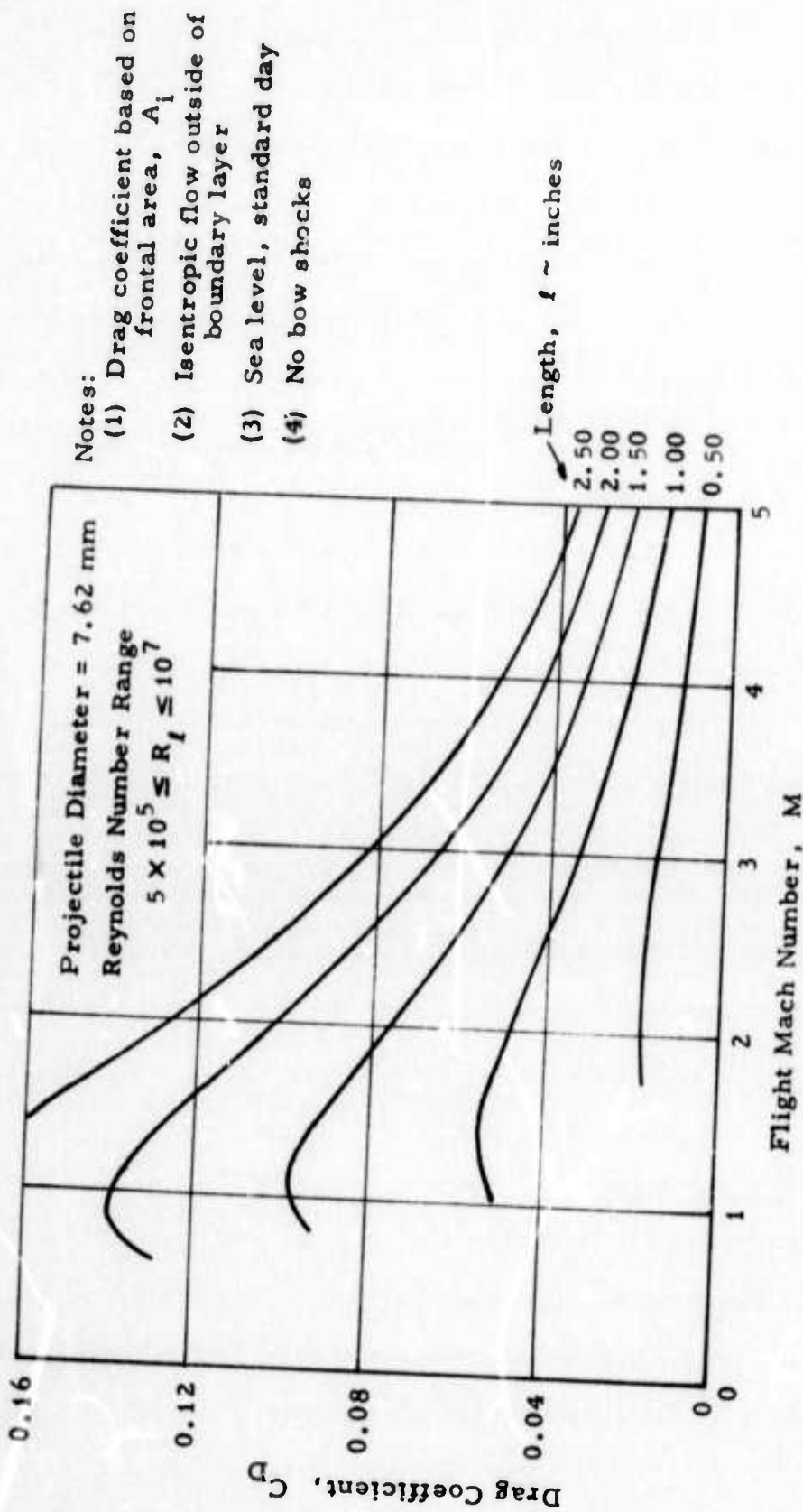
b. Experimental Confirmation

The experimental confirmation of low drag was first established via wind tunnel testing which assessed the character of the flow field using Schlieren techniques. This study showed that the flow entered and exited smoothly from the model in the design operating regime. Only weak waves indicative of small losses and low drag were detected.

For additional confirmation, a three-component force balance was employed to directly measure lift, moment, and drag characteristics. The drag measurement yielded values of $C_D \approx 0.05$ at Mach numbers of $3 < M < 4$ which is in general agreement with the theoretically predicted values of Fig. 4.

2. Wide Operating Range

Hollow projectiles can be designed to operate efficiently (low drag) over a very wide range of velocities and distances. Conditions establishing the boundaries of this high performance region were first analytically established (Ref. 4) and then experimentally confirmed via wind tunnel testing (Ref. 5).



EFFECT OF LENGTH AND SPEED ON DRAG COEFFICIENT
 7.62 mm Hollow Projectiles

Fig. 4

a. High Performance Region

The hollow projectile must first be launched with a sufficiently high muzzle velocity to allow "swallowing" of the bow shock and the establishment of smooth supersonic flow inside the projectile. Then as the projectile slows down the flow inside the projectile "chokes" and the bow shock with its associated high drag appears.

Basically, the hollow projectile is composed of an internal compression inlet, a throat section, and a nozzle. Internal compression inlets require special attention to the so-called "starting problem," i.e., the problem of initially swallowing the bow shock.

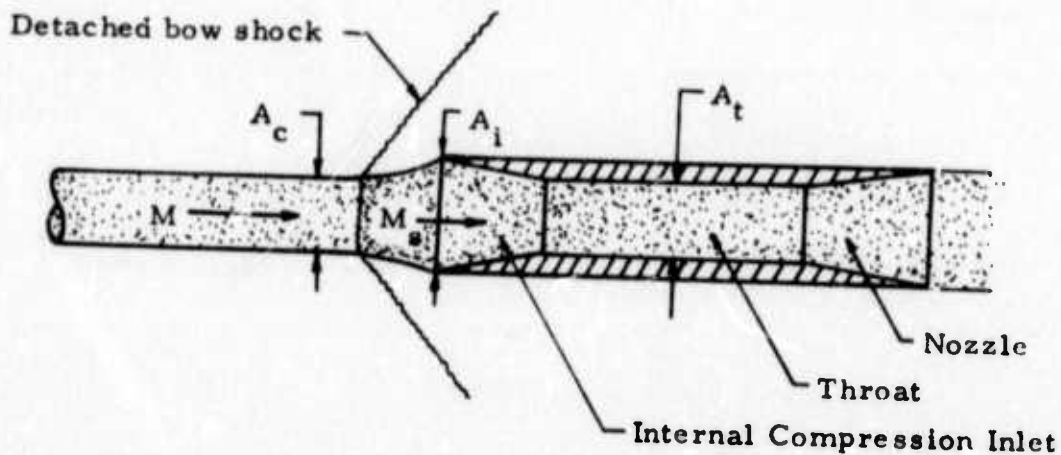
As a hollow projectile leaves the muzzle of a rifle, there is no flow through the projectile. The projectile is equivalent to a blunt body and thus there is a bow shock. When the projectile separates from its sabot, air can flow through the internal passage in the projectile. If the passage is sufficiently large, the bow shock will be "swallowed" and essentially disappear. Then, if flow separations and other such potential sources of loss (energy dissipation) are avoided, low drag as predicted in Fig. 2 can be achieved.

(1) Theoretical basis

The starting problem is well-known. A concise summary analysis is given in Ref. 6. Much of the basic work was originally accomplished in Refs. 7 and 8. A simplified summary presentation will now be given to delineate the basic features in the analysis which specifically guided design and experimental activities presented in this report.

The character of the starting problem is easily visualized by first considering the case where the internal passage is too small. There

will then be a detached bow wave in front of the hollow projectile as illustrated below.



The upstream capture area A_c is less than the inlet area A_i , i.e., $A_c < A_i$. Here, the captured flow is defined as the flow (stream tube) that passes through the hollow projectile.

The portion of the detached shock that cuts across the captured stream tube is approximated as a straight vertical shock and is therefore treated as a normal shock. The Mach number downstream of this normal shock is subsonic and is denoted by the symbol M_s . The upstream Mach number is M .

For approximate estimation purposes, the boundary layer on the surface of the projectile can be disregarded. Corrections for boundary layer effects can be introduced as a refinement. The primary effect of the boundary layer is to reduce the "effective" size of the internal passage. That is, the internal wall friction (manifest as the boundary layer) will tend to reduce the mass flow rate through the projectile.

The present analysis focuses on configurations where boundary layer effects are not dominant. The subsonic captured flow downstream of the normal shock (see previous sketch) can then be regarded as an essentially isentropic flow. As this flow approaches the throat (minimum internal passage diameter) it speeds up and reaches sonic speed at the throat. The flow is then "choked" and the mass flow rate is limited by the size of the throat as denoted by A_t .

It clearly follows that the upstream capture area A_c and the throat area A_t are related. If A_t is increased, the internal mass flow increases and A_c must also increase from continuity considerations. For isentropic flow of a perfect gas, the areas are related as follows (Ref. 6)

$$\frac{A_c}{A_t} = \frac{1}{M_s} \left[\frac{2}{\gamma+1} \left(1 + \frac{\gamma-1}{2} M_s^2 \right) \right]^{\frac{\gamma+1}{2(\gamma-1)}} \quad (3)$$

where γ is the ratio of specific heats.

Further, for the normal shock in the captured stream tube, the downstream Mach number M_s is simply related to the upstream Mach number M , i.e.,

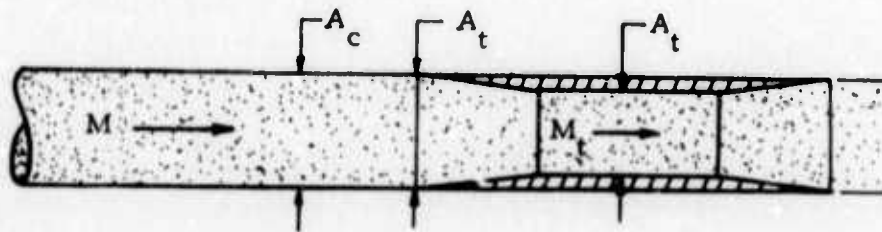
$$M_s = \left\{ \frac{\frac{2}{(\gamma-1)} + M^2}{\frac{2\gamma}{(\gamma-1)} M^2 - 1} \right\}^{1/2} \quad (4)$$

where $M \geq 1$. When $M = 1$, it is readily found from Eq. (4) that $M_s = 1$.

From Eq. (4) it is clear that when the flight speed M is chosen, the value of M_s is determined. Then from Eq. (3), the ratio of A_c/A_t is established. Thus, if the throat area A_t is increased, the capture area A_c will be increased by the same factor. If A_t and hence A_c

are increased, the detached bow shock (see sketch) moves downstream. When A_c becomes equal to the inlet area A_i , the bow shock is located at the inlet face. A further incremental increase in A_t will cause the bow shock to move through the projectile.

At this point, the flow has been successfully started. The detached bow shock has been eliminated. The internal flow in the projectile is supersonic and the Mach number in the throat is greater than sonic, i.e., $M_t \geq 1$. The desired high performance flight operating condition is illustrated below.



For small boundary layer effects and shallow bevel angles, the flow in the captured stream tube can be approximately treated as supersonic one-dimensional isentropic flow. For this type of flow, it is readily deduced that

$$\frac{A_c}{A_t} = \frac{A_i}{A_t} = \frac{M_t}{M} \left[\frac{(1 + \frac{\gamma-1}{2} M^2)}{(1 + \frac{\gamma-1}{2} M_t^2)} \right]^{\frac{\gamma+1}{2(\gamma-1)}} \quad (5)$$

where A_t is chosen to be sufficiently large to allow starting as described earlier.

After the projectile had started, it will gradually lose speed, i.e., M will decrease. Since the ratio (A_c/A_t) is fixed, there will be a corresponding decrease in M_t as governed by Eq. (5). Here, M_t

is initially greater than one and gradually approaches the sonic or choked condition of $M_t = 1$ as the flight speed decreases.

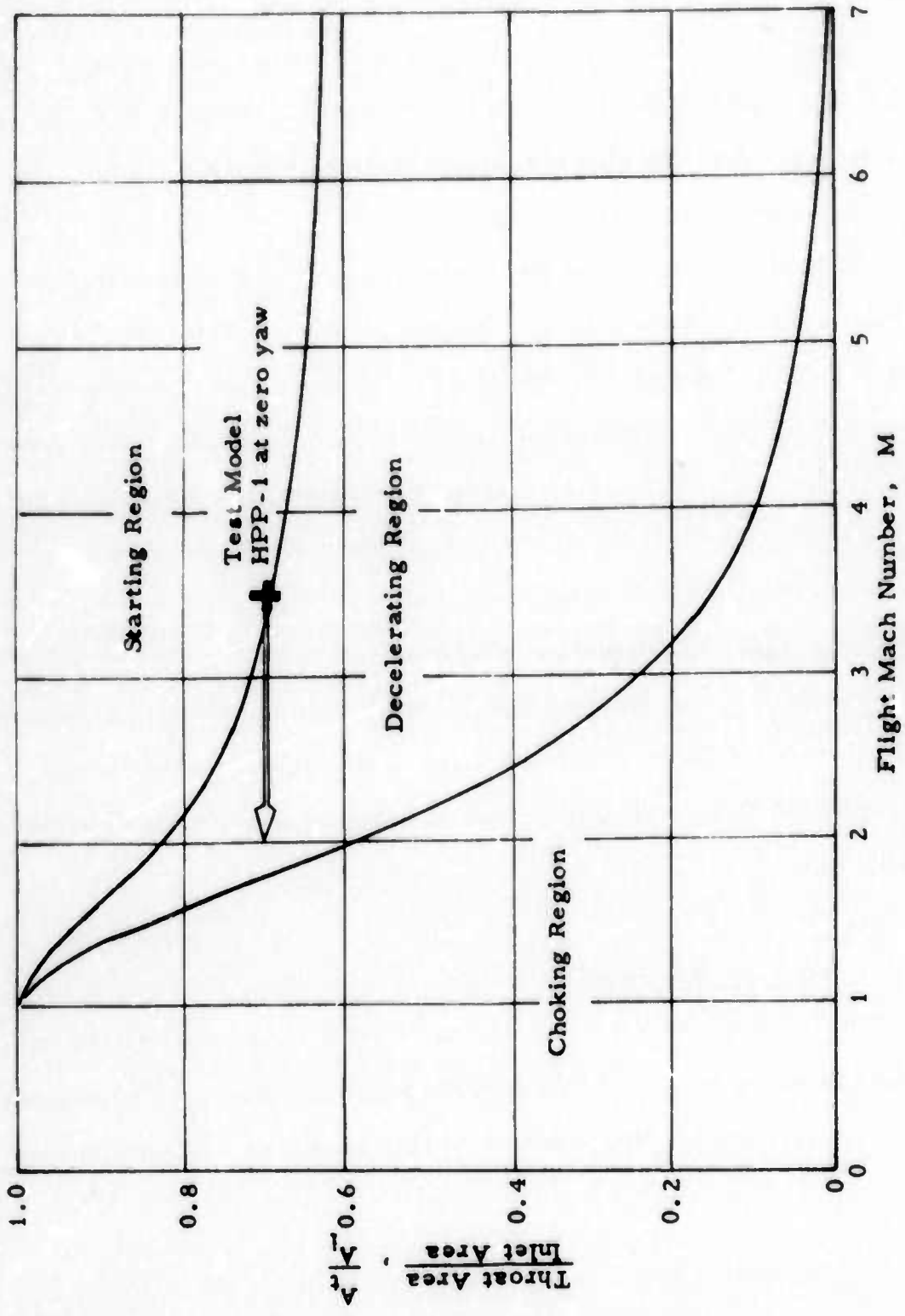
After the choked condition is reached, further decreases in flight speed will result in the formation of a bow shock wave. Performance will then be degraded. Thus, the regeneration of the bow shock wave denotes the end of high performance flight.

This high performance flight zone consisting of a 'starting' and 'decelerating' region is shown in Fig. 5. The ratio of throat area to inlet area is shown as a function of flight Mach number. As the throat size (ratio of A_t/A_i) decreases, a higher starting velocity is required. For values of $(A_t/A_i) < 0.7$, starting velocity requirements increase very rapidly. That is, there is a knee in the curve at $(A_c/A_i) \approx 0.7$ and $M \approx 3.5$. This knee corresponds to a configuration which is a reasonable starting point for preliminary design trade-off studies.

Normally, it is expected that the projectile will be designed so that it will impact the target while operating in the high performance decelerating region of Fig. 5. The present investigation is therefore concentrated on this region.

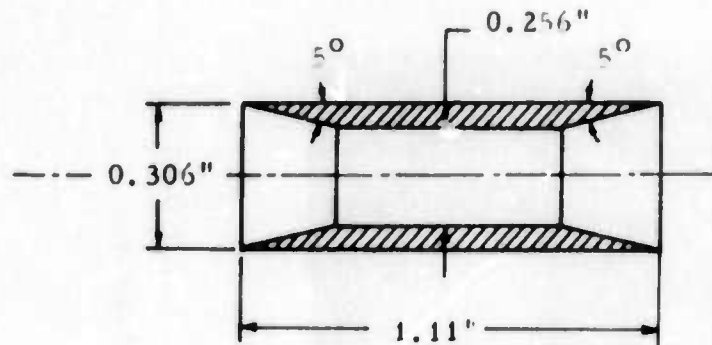
(2) Test Verification

The existence of a wide operating velocity range was demonstrated in wind tunnel testing. For this purpose, a simple basic model designated HPP-1 was selected. The geometry of this projectile is shown below.



HOLLOW PROJECTILE OPERATING REGION

Fig. 5



The projectile is 30-caliber (7.62 mm) with a cylindrical exterior. Interior taper angles of 5 degrees are used both at the front and rear of the model.

The region of high performance, low drag flight was determined via Schlieren techniques. In the high performance region, the projectile is launched with sufficient speed (Mach 3.5) to start with no bow shock. As the speed decays, a bow shock eventually appears. This bow shock is associated with a sharp drag rise and thus its occurrence terminates high performance flight.

Schlieren results supporting the above findings are presented in Fig. 6. The "initial" and "final" conditions shown on Fig. 6 correspond to the end points of the high performance operation of HPP-1 shown on Fig. 5. At the initial condition ($M = 3.5$) the photograph clearly shows that there is no bow shock. At the final condition a bow shock is clearly seen.

The experimentally determined high performance region for test model HPP-1 is in close agreement with theoretical predictions as shown in Fig. 5. The test model choked slightly sooner (Mach 2) than the theoretical prediction (Mach 1.8). But this slight discrepancy is



Initial Condition: $M = 3.5$
(No Bow Shock)



Final Condition: $M = 2.0$
(Bow Shock Appears)

DETERMINATION OF HIGH PERFORMANCE REGION

Schlieren Photographs of HPP-1 at Zero Yaw

Fig. 6

explainable in terms of viscous boundary layer effects which were not incorporated in the idealized theory.

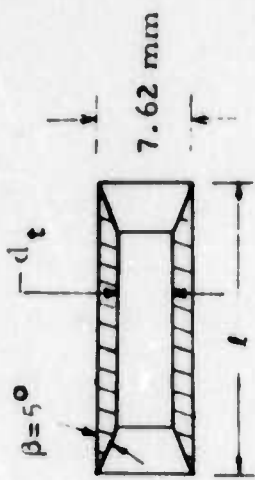
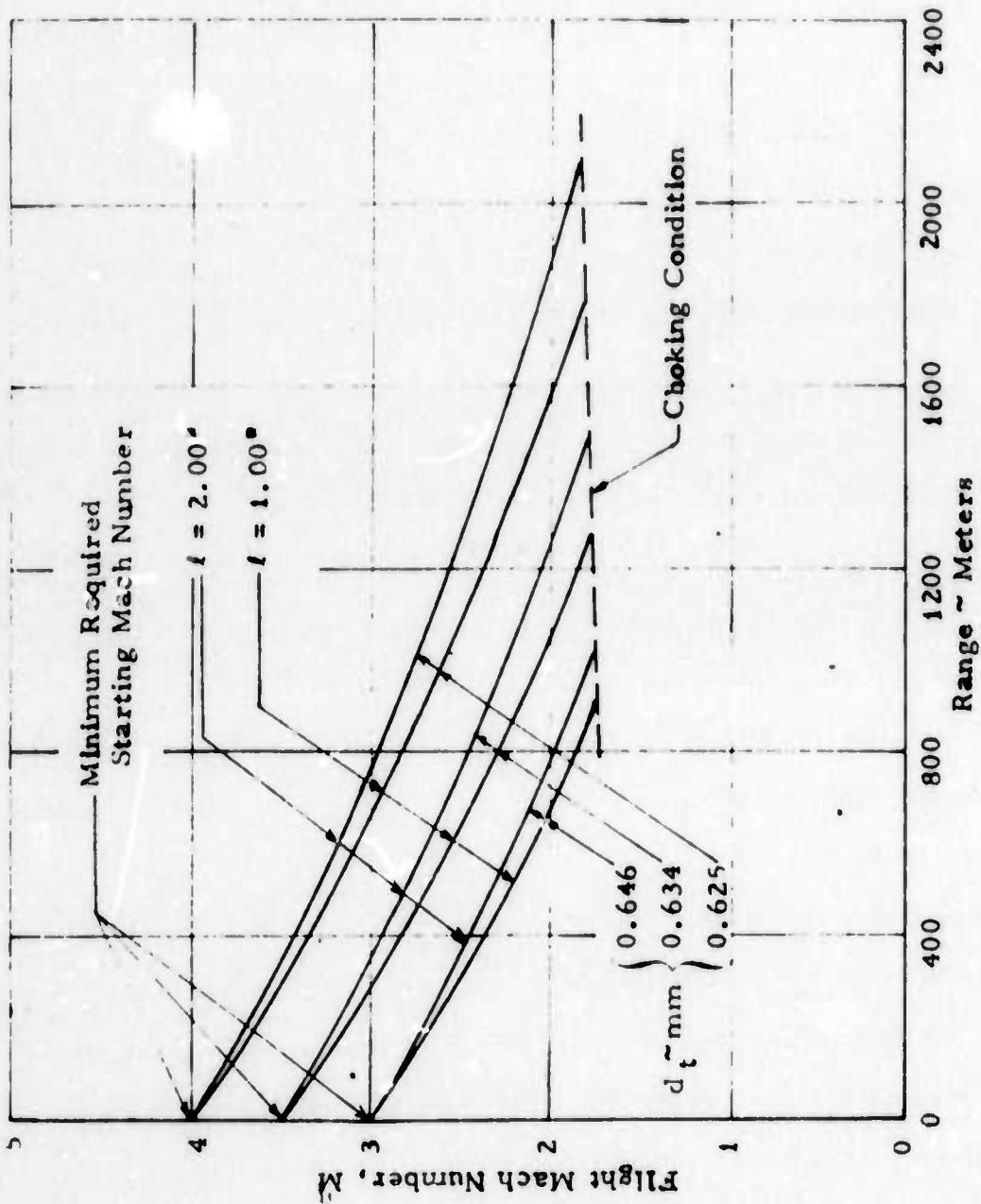
The wide velocity range shown in Fig. 5 corresponds to efficient flight over a long distance. These distances generally exceed 1000 meters as shown in Fig. 7. A spectrum of configurations are presented on Fig. 7 to show that hollow projectiles can be readily tailored to specific requirements. In general, the highest launch velocity achievable within interior ballistic constraints of the selected weapon produces the highest range and best performance. Straightforward details regarding construction of Fig. 7 are presented in Ref. 9.

Firing range tests have demonstrated that launch velocities in excess of Mach number equal to 3.5 can be achieved using a standard 7.62 mm cartridge and barrel. The projectiles were fired with the aid of a simple plug sabot at the base. This shows that the demonstrated high performance can be achieved in an actual weapons system.

b. Stable Flight Characteristics

The hollow projectile must possess stable flight characteristics to successfully operate in the high performance region described above. This can be provided via spin-stabilization as employed in conventional weapons systems.

Rifling in the barrel can communicate spin to the sabot which in turn spins the projectile. Alternatively, the spin can be imparted directly to the projectile via a thin soft metal or plastic coating bonded to the outer surface of the projectile. This latter method is commonly used in conventional small arms applications and was successfully applied to 7.62 mm hollow projectiles investigated in this program.



Projectile Material: Steel

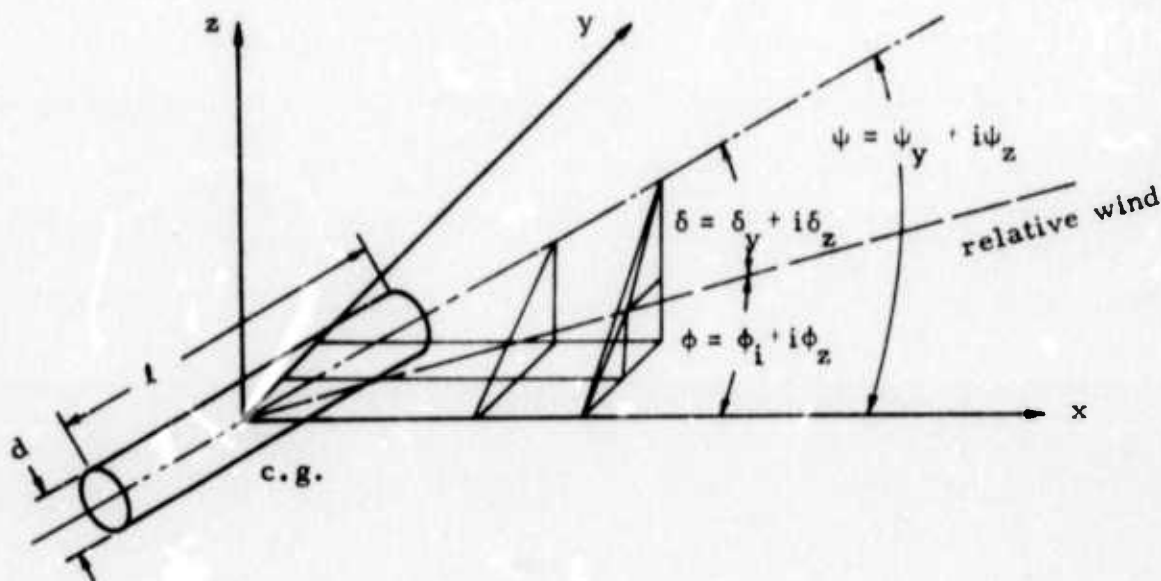
HOLLOW PROJECTILE RANGE
Velocity Decay Characteristics in High Performance Region

Fig. 7

(1) Basic Stability Criteria

Basic analytical criteria concerning spin stability are well-known. These criteria (as detailed in Ref. 4) have been applied to hollow projectiles.

Consider a projectile in three-dimensional space with reference axes and angles as shown in the sketch below



where the two-dimensional vector quantities in the y - z plane are expressed in the form of complex variables.

The equations of motion for five degrees of freedom (including overturning moment, damping and magnus moments, and spin rate) can be expressed as the following ordinary differential equation,

$$\begin{aligned}
I_b \ddot{\delta} + \left(\frac{I_b C_l}{2m} \rho AV + C_q \frac{\rho}{2} Al^2 V - i I_a N \right) \dot{\delta} \\
+ \left(\frac{C_q C_l}{4m} \rho^2 A^2 l^2 V^2 - \frac{I_b C_D C_l}{4m^2} \rho^2 A^2 V^2 \pm i K_j \rho d^4 NV \right. \\
\left. - C_m \frac{\rho}{2} Al V^2 - i I_a N \frac{C_l}{2m} \rho AV \right) \delta = 0 \quad (6)
\end{aligned}$$

where

I_a = mass moment of inertia about body longitudinal axis

I_b = mass moment of inertia about a transverse body axis through the c.g.

N = spin rate in rad/sec about the longitudinal axis of the body

C_q = damping moment coefficient

ρ = air density

A = cross sectional area of body

l = body length

V = velocity

K_j = magnus moment coefficient, "+" sign for a c.p. forward of the c.g., and "-" for a c.p. aft of the c.g.

C_m = slope of overturning moment coefficient positive for unstable moment. (c.p. is ahead of c.g.) $C_m = (dC_M/d\delta)$

m = total mass

C_l = slope of lift coefficient versus δ ($C_l = dC_L/d\delta$)

C_D = drag coefficient

The solution of Eq. (6) is in the form of $\delta = e^{\lambda t}$. The stability and damping characteristics of the projectile can be obtained by examining the value of λ , i.e., Real (λ) ≥ 0 for harmonic or damped motion.

Considering only the overturning moment for a spin stabilized

projectile it can be shown that the following inequality must be satisfied if stable operation is to be realized,

$$- I_a^2 N^2 + 4 L_b C_m \frac{\rho}{2} A l V^2 < 0 \quad (7)$$

Now consider a hollow cylinder projectile and note that

$$I_a = m \frac{r^2 + r_i^2}{2} \equiv m r_a^2 \equiv K_a^2 m r^2$$

where r = outside radius, r_i = inside radius, and r_a is the radius of gyration. Similarly, define

$$L_b \equiv K_b^2 \frac{m l^2}{12}$$

and note that

$$m = \rho_m 2\pi K_m r t l$$

where $t = r - r_i$, ρ_m = mass density of the projectile, and $K_m = (r + r_i)/2r$ for a straight cylinder.

Then, for a stable projectile the following condition [see Eq. (7)] must be satisfied

$$\left(\frac{N r}{V} \right)^2 > \frac{K}{3} \frac{\rho}{\rho_m} C_m \left(\frac{l}{r} \right) \left(\frac{l}{d} \right)^2 \quad (8)$$

where

$$K = \frac{K_b^2}{K_a^4 K_m}$$

For a slender, thin-walled projectile, $K \approx 1$, and if the projectile is made of steel, $\frac{\rho}{\rho_m} = 1.65 \times 10^{-4}$. Then, assuming a typical value of

$t/r = 0.2$, it follows that

$$\left(\frac{Nr}{V}\right)^2 > 2.75 \times 10^{-4} C_m \left(\frac{l}{d}\right)^2$$

and the twist requirement is

$$\text{twist} = \frac{1}{V} \frac{N}{2\pi r} = \frac{1}{2\pi r} \left(\frac{Nr}{V}\right) \quad (9)$$

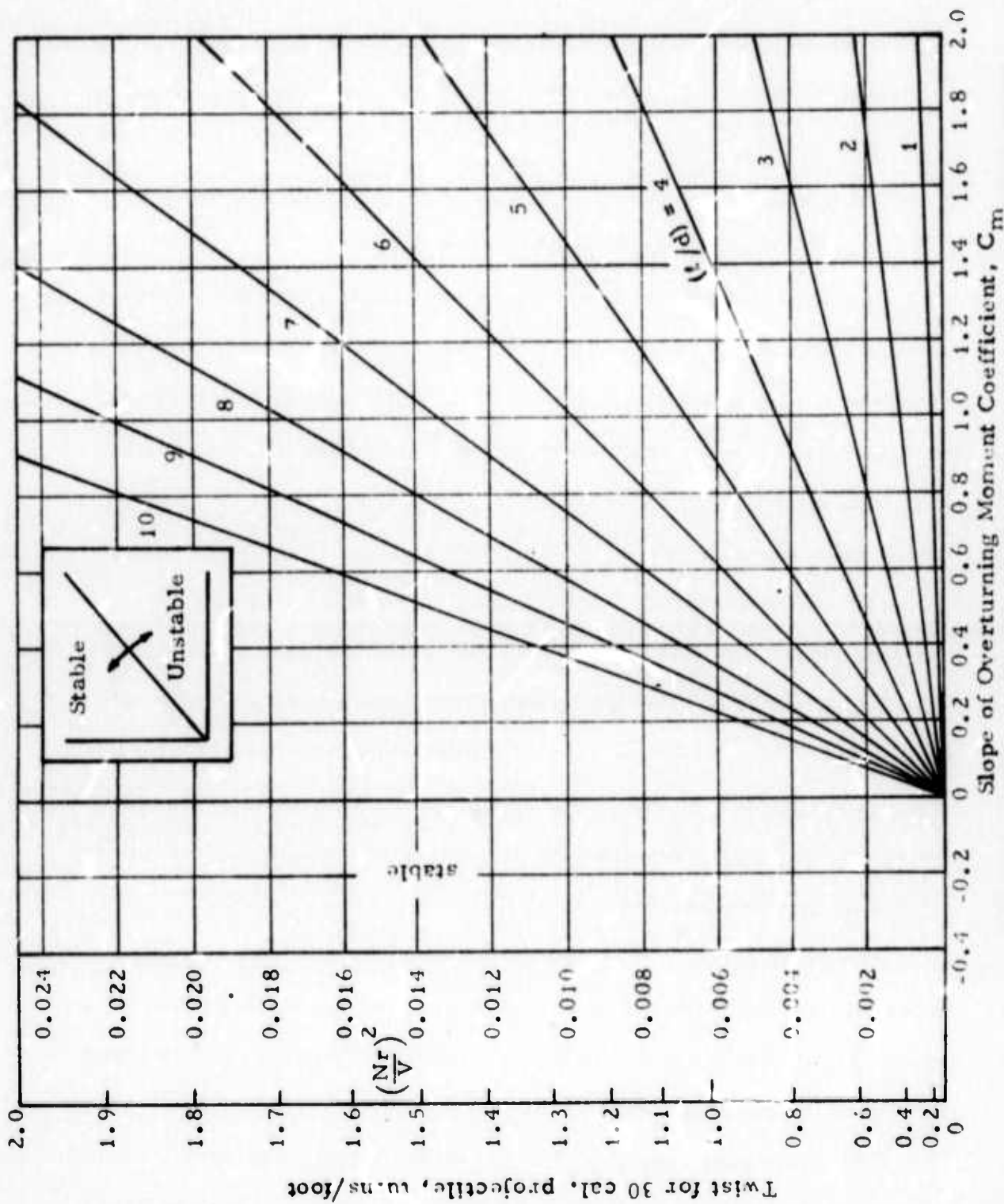
This result is shown in Fig. 8. Basically, spin rate (or twist) is presented as a function of the slope of the overturning moment coefficient C_m with the projectile length to diameter ratio (l/d) as a parameter.

Consider, for example, the curve (straight line) corresponding to a length/diameter ratio of (l/d) = 3.0. If the projectile operates in the region beneath this line, it will be unstable. For operation above the line it will be stable. Thus, the lines of Fig. 8 are essentially separation lines between stable and unstable operating regimes.

Selection of the basic geometry and mass distribution of a particular projectile essentially fixes (l/d) and C_m . The spin rate required for stability can then be read directly from Fig. 8. As expected higher spin rates provide greater stability.

The desirability of achieving low values for the slope of the overturning moment coefficient is also clearly evident. For low values of C_m , low spin rates are required to achieve stability. In fact if $C_m \leq 0$, stability can be attained without spinning. Thus, one clear design objective is to obtain the lowest possible value for C_m via a combination of aerodynamic shaping and mass distribution.

A further trend shown in Fig. 8 is that projectiles with high length/diameter ratios will rely more critically on achievement of low



STABILITY BOUNDARIES OF SPIN STABILIZED HOLLOW PROJECTILES

Fig. 8

values for the slope of the overturning moment coefficients. For a given C_m , projectiles with higher values of (l/d) require greater spin rates as clearly seen from Fig. 8. Excessive spin rates can be avoided by providing low C_m values.

(2) Aerodynamic Considerations

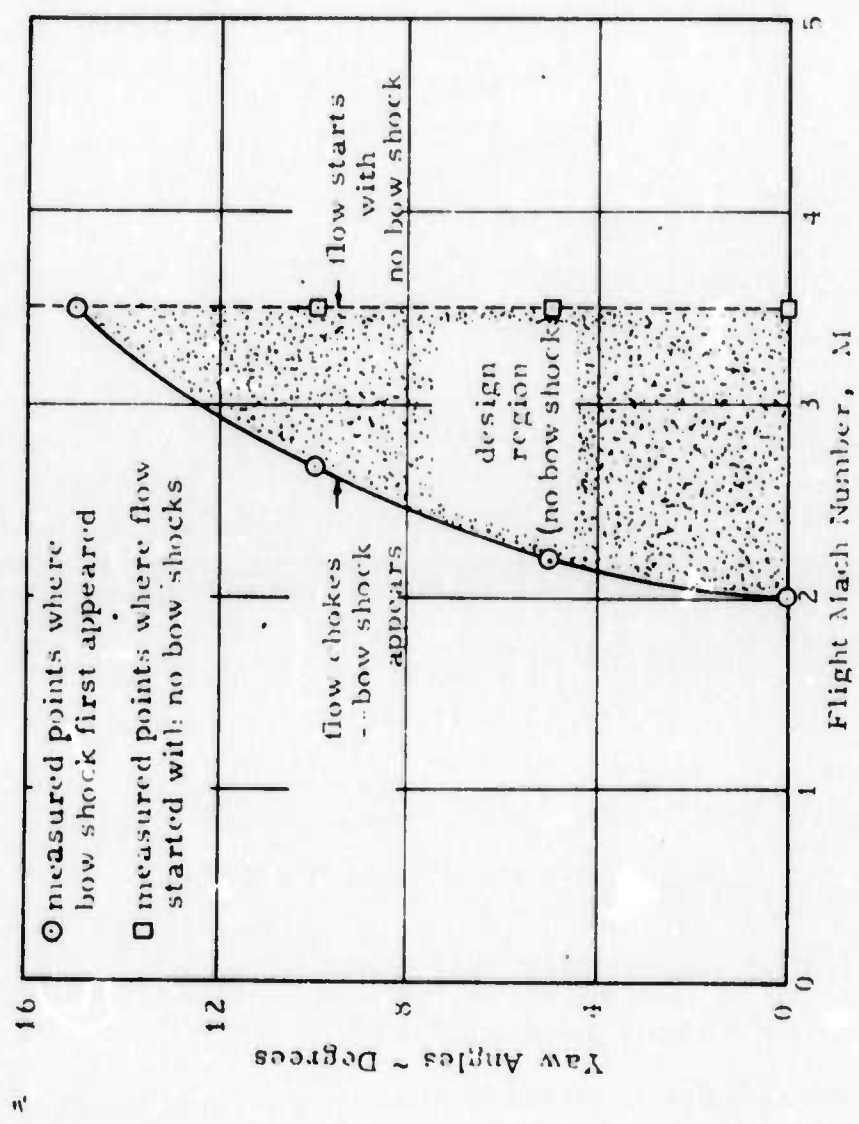
The aerodynamic force and moment changes associated with yawing motions of the projectile are of paramount importance as exemplified by the effect of C_m shown in Fig. 8. From flow field considerations, large yaw angles will induce adverse flow phenomena such as separated flow regions and shock wave formation.

These adverse phenomena increase drag and reduce the high performance operating region. The limits on yaw angle to avoid these adverse effects was established via wind tunnel testing.

From model HPP-1, yaw effects were assessed via Schlieren techniques. The model was yawed to a selected angle and a test run was conducted at the previously reported (Figs. 5 and 6) starting condition of $M = 3.5$. If the flow were smooth with no bow shock, the speed was reduced until a bow shock appeared.

The results of this testing are shown on Fig. 9. As the yaw angle increases, the bow shock appears sooner. That is, the high performance region becomes narrower. At a yaw angle of 15 degrees, a bow shock appears at the starting speed of $M = 3.5$.

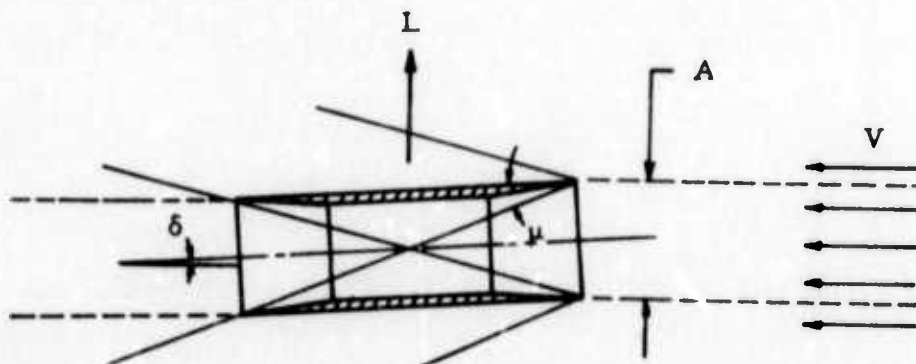
For yaw angles less than 5 degrees the degradation appears small. Thus, as a design goal (at least for HPP-1), it would be desirable to provide sufficient stability to limit the nominal yaw variations to less than 5 degrees.



EFFECT OF YAW ON HIGH PERFORMANCE REGION
 Test Model HPP-1

Fig. 9

The lift and moment characteristics of hollow projectiles can be analytically estimated for small yaw angle variations where large adverse flow field effects are not encountered. Consider a general hollow projectile as sketched below,



The lift force L (normal to the flight direction) is comprised of contributions from (1) turning the internal flow and (2) the cross-flow associated with the external flow.

For small yaw angles ($\delta \ll 1$), the lift force contributed by the internal flow is

$$L_{\text{int}} = \dot{m}(V \sin \delta) \approx \rho AV^2 \delta \approx 2A\delta q \quad (10)$$

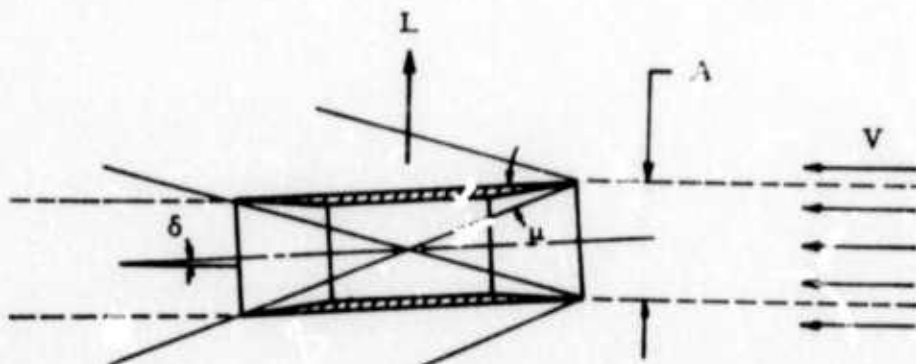
where A is the cross sectional area of the internal flow (see sketch) and $q = \frac{1}{2} \rho V^2$ is the dynamic pressure.

The external flow contribution due to cross-flow can be estimated from slender body theory (Ref. 10), i.e.,

$$L_{\text{ext}} = 2A\delta q \quad (11)$$

where it is noted that $L_{\text{int}} = L_{\text{ext}}$.

The lift and moment characteristics of hollow projectiles can be analytically estimated for small yaw angle variations where large adverse flow field effects are not encountered. Consider a general hollow projectile as sketched below,



The lift force L (normal to the flight direction) is comprised of contributions from (1) turning the internal flow and (2) the cross-flow associated with the external flow.

For small yaw angles ($\delta \ll 1$), the lift force contributed by the internal flow is

$$L_{int} = \dot{m}(V \sin \delta) \approx \rho AV^2 \delta \approx 2A\delta q \quad (10)$$

where A is the cross sectional area of the internal flow (see sketch) and $q = \frac{1}{2} \rho V^2$ is the dynamic pressure.

The external flow contribution due to cross-flow can be estimated from slender body theory (Ref. 10), i.e.,

$$L_{ext} = 2A\delta q \quad (11)$$

where it is noted that $L_{int} = L_{ext}$.

The lift coefficient is then

$$C_L \equiv \frac{L}{qA} = \frac{L_{int} + L_{ext}}{qA} = 4\delta \quad (12)$$

The corresponding lift-curve slope is $C_{L_t} = (\partial C_L / \partial \delta) = 4 = 0.0697/\text{deg}$.

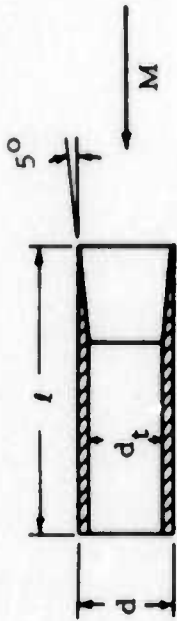
Based on the flow field, the external force acts near the mid-length. For speeds of $M \approx 3.5$ and projectile length/diameter ratios (l/d) of about 3 or less, the internal force also will act at approximately mid-length. This is inferred by noting that the Mach wave angle for $M = 3.5$ is $\mu = 16.6^\circ$ (see sketch).

When the internal flow waves from one surface do not impinge and reflect from the opposite surface, the internal flow force will essentially act at the midpoint for symmetrical inlet and exit bevel configurations. To first order, the waves will not impinge if $(l/d) < \cot \mu = \cot 16.6^\circ \approx 3$.

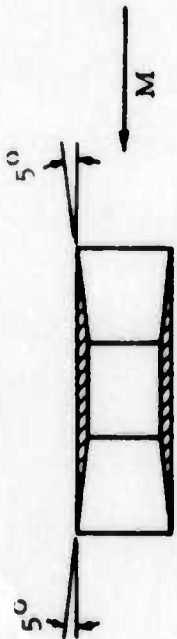
The three-dimensional internal flow is actually very complex, particularly when boundary layer effects are considered. However the basic character of the flow is portrayed by the general first order considerations discussed above.

Wind tunnel force balance tests were conducted on a series of related models encompassing ten (10) configurations. Lift coefficient test data for configurations M-5 and M-7 are presented in Fig. 10 as a function of yaw angle. These data are in reasonably close agreement with the analytically estimated lift-curve slope, particularly for small yaw angles.

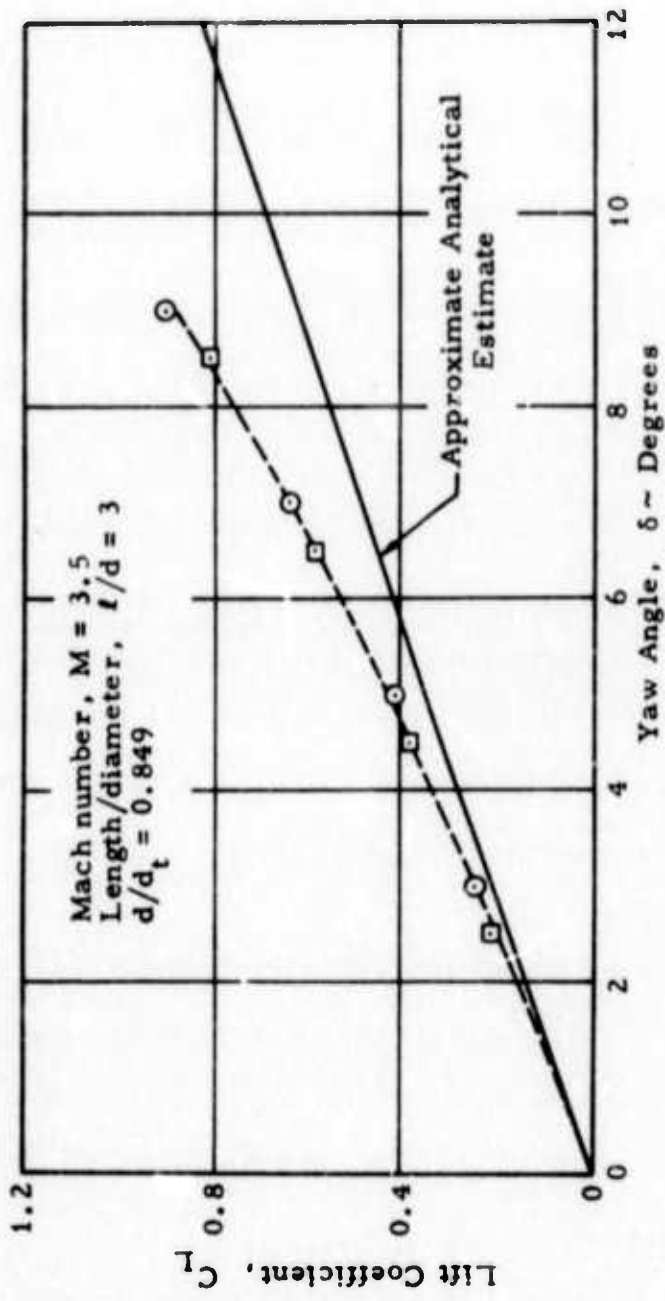
The present wind tunnel force tests were designed to ascertain basic trends and overall force and moment levels. Possible sources of error include model support tare corrections, deflection of the



⊙ - Configuration M-5



⊠ - Configuration M-7



EXPERIMENTAL LIFT CURVE SLOPE

Fig. 10

cantilever model support strut, and test section flow angularities.

Elimination or minimization of these secondary sources of error would be extremely tedious and could not be justified for present program objectives.

For test model configuration M-5, it was ascertained from analysis of the lift and moment test data that the center of pressure c.p. is approximately located between 33% and 55% of the length from the leading edge. This generally confirms the analytical estimate of 50% discussed previously.

In firing range tests, the projectile will be spinning and this introduces some (probably secondary) aerodynamic effects. For this reason, wind tunnel effort was limited to acquiring only approximate bounds on parameters such as c.p. The function of this data was to provide guidance for the firing range test program where the projectile is evaluated under completely realistic operating conditions.

(3) Firing Range Test Results

The firing range tests initially concentrated on short range tests aimed primarily at developing a simple "workhorse" plug sabot to cleanly launch the projectile. Then tests indicating potential for high accuracy and low dispersion were conducted.

Firing results on selected configurations indicate that accuracy and dispersion are very sensitive to small changes in geometrical parameters. Continued development testing is required to isolate the critical factors. This activity should be highly productive since the high sensitivity infers that the projectiles can be optimized and thereby

achieve accuracy and dispersion results considerably better than those presently obtained.

Results which illustrate this point are provided on the attached charts (Figs. 11 through 13). Note that all the projectiles are basically similar except for small geometrical differences. Further, P-96 (Fig. 12) has a polypropylene coating while P-93 (Fig. 11) and P-97 (Fig. 13) have a copper coating. Results indicate that the copper coating provides greatly improved accuracy and dispersion characteristics.

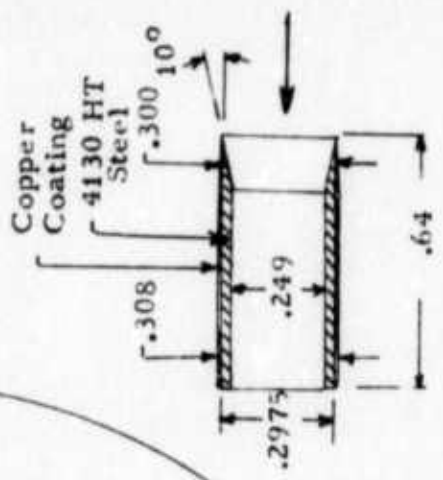
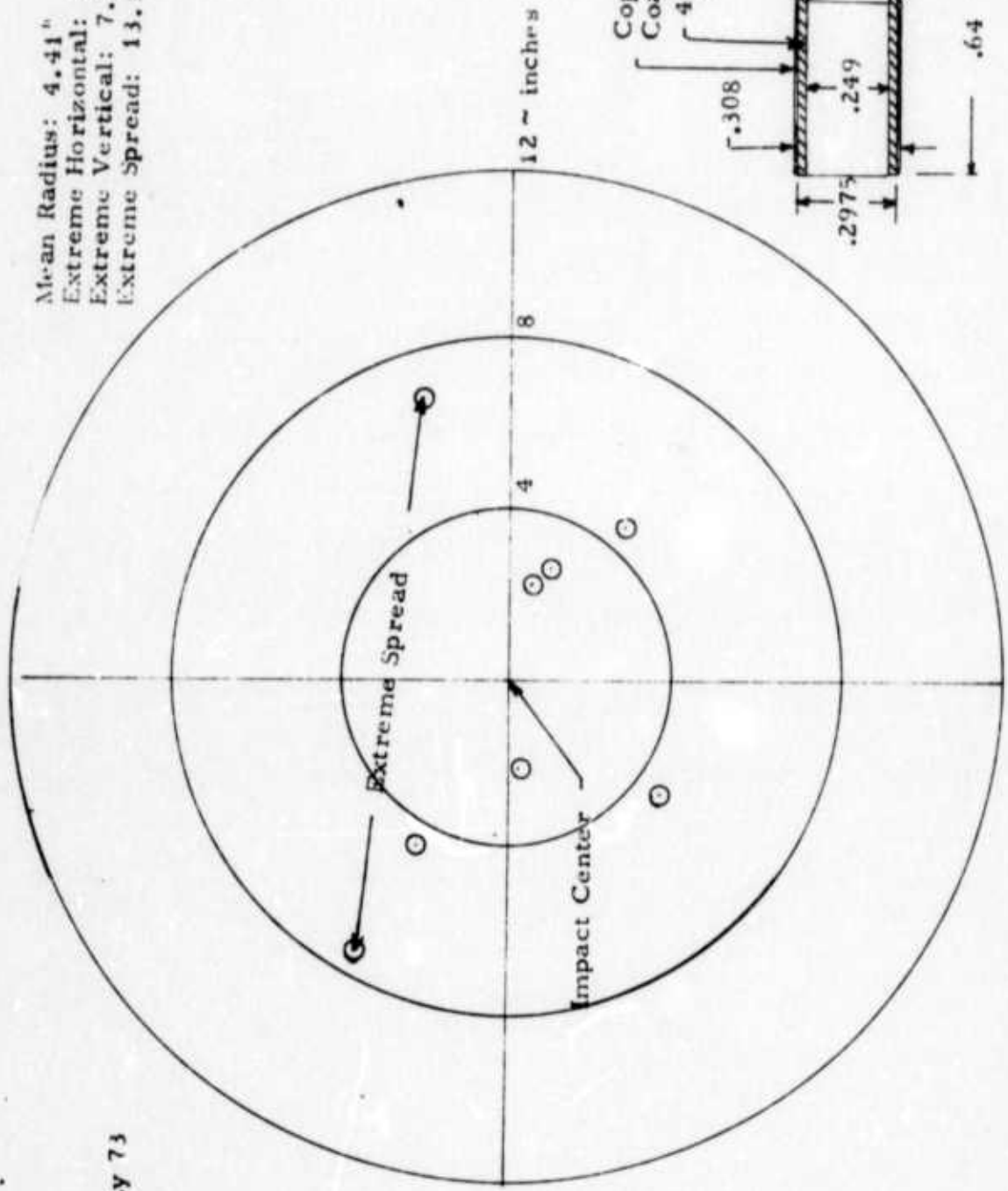
Possible explanations are that the copper coated projectiles are slightly heavier. Or, perhaps the polypropylene coating is roughened up in the barrel which results in degradation of aerodynamic characteristics. Differences in fabricating techniques might have resulted in slightly better concentricity for copper coating projectiles. The c.g. of the lighter polypropylene coating projectiles (P-96) is slightly more forward than P-93 but this should have improved stability.

The chart for projectile P-97 with a copper coating provides results generally comparable to the other copper coated projectile, P-93. However, P-97 has a bevel at the rear and concentric grooves in the coating at the left portion. This moves the c.g. forward while slightly decreasing the weight. The benefits of a forward c.g. shift could possibly have been off set by weight reduction or aerodynamic effects of the concentric grooves.

Short range firings at a distance of 15' to 20' indicate that the selected projectiles had essentially zero yaw in this short distance. Longer and heavier projectiles exhibited varying degrees of yaw in this short distance. It is conceivable that short range yawing motions of

Projectile: P-93
 Sabot: S-61
 Firing Date: 11 May 73
 Muzzle Velocity:
 5480-5610 fps
 Gusty Winds:
 0 - 20 mph

Mean Radius: 4.41"
 Extreme Horizontal: 13.10"
 Extreme Vertical: 7.39"
 Extreme Spread: 13.19"

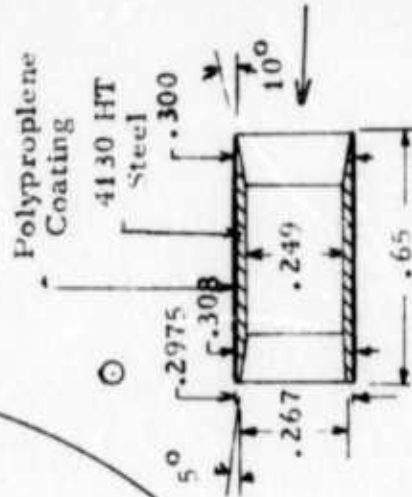
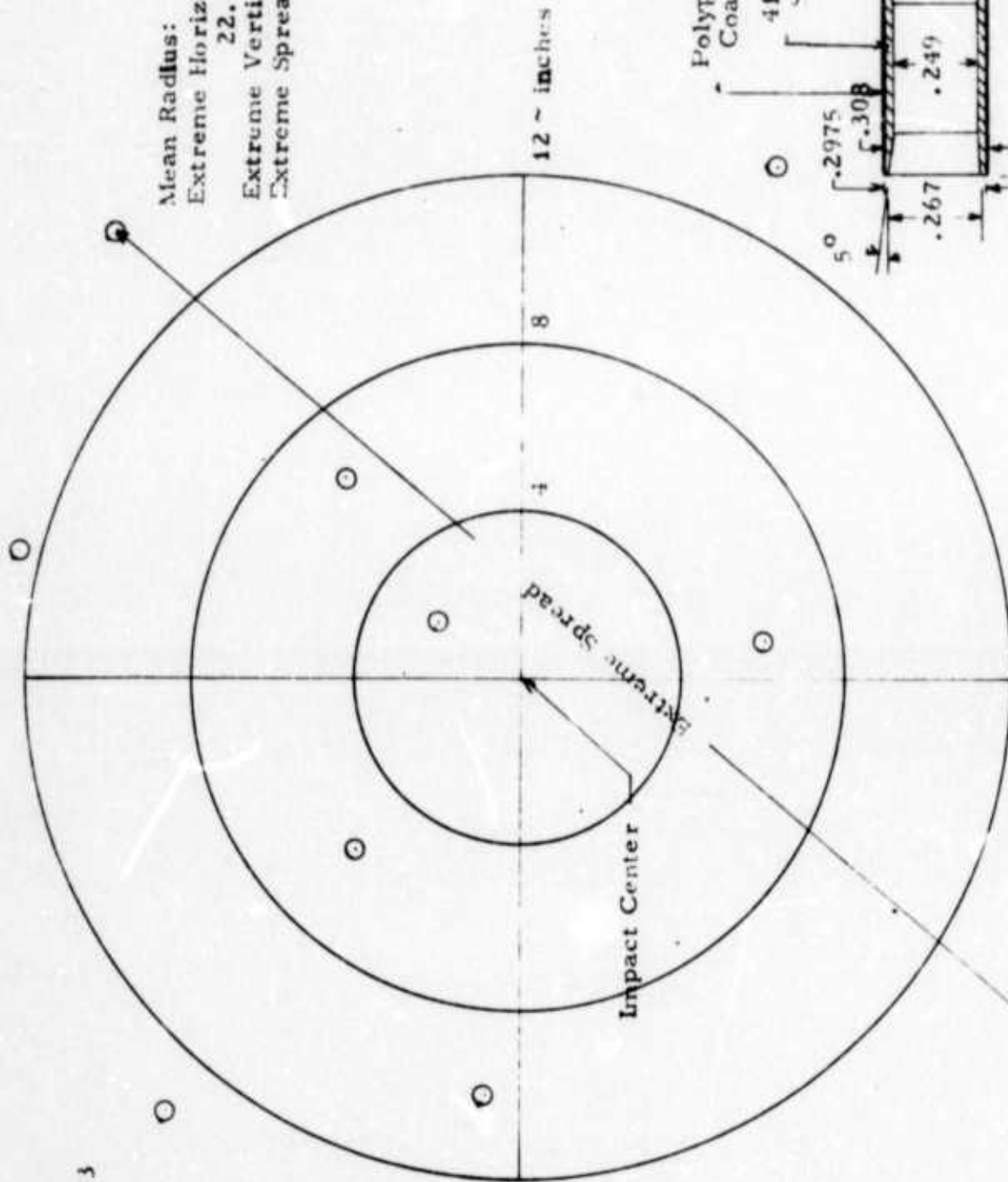


ACCURACY AND DISPERSION TEST RESULTS
 Projectile P-93; Target: 555'

Fig. 11

Projectile: P-96
 Sabot: S-62
 Firing Date: 15 May 73
 Muzzle velocity:
 5650-5875 feet
 Gusty winds:
 0 - 20 mph

Mean Radius: 10.13"
 Extreme Horizontal:
 22.46"
 Extreme Vertical: 26.43"
 Extreme Spread: 30.06"

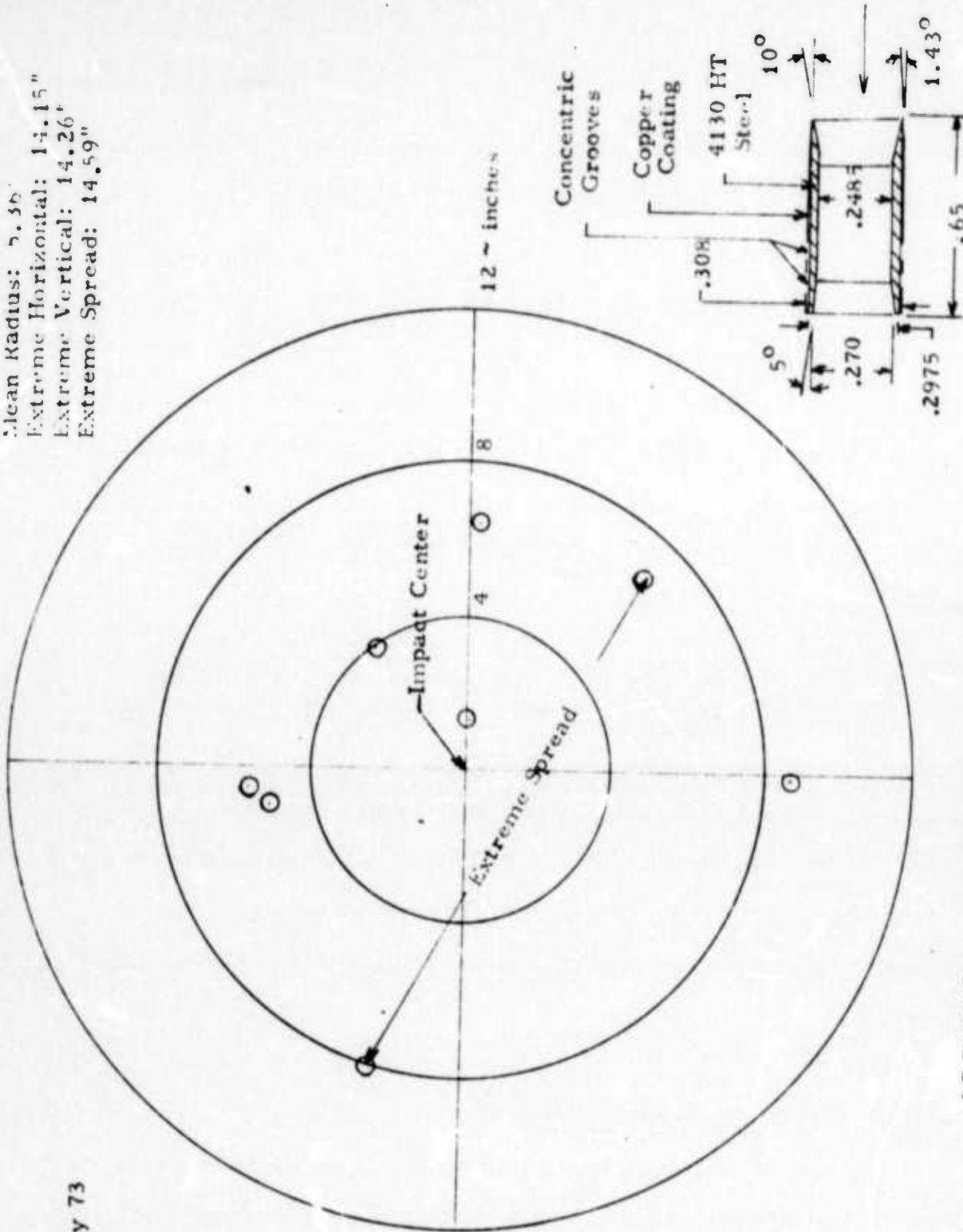


ACCURACY AND DISPERSION TEST RESULTS
 Projectile P-96; Target: 555'

Fig. 12

Projectile: P-97
 Sabot: S-62
 Firing Date: 18 May 73
 Muzzle Velocity:
 5500-5650 fps
 Gusty winds:
 0 - 20 mph

Mean Radius: 5.56'
 Extreme Horizontal: 14.15"
 Extreme Vertical: 14.26"
 Extreme Spread: 14.59"



ACCURACY AND DISPERSION TEST RESULTS
 Projectile P-97; Target: 555'

Fig. 13

the longer and heavier projectiles would damp out with distance and that these projectiles would provide better accuracy and dispersion characteristics for long range firing.

The desirability of conducting additional firing tests during follow-on phases is clearly indicated. However, the present tests clearly demonstrate that hollow projectiles can be effectively spin-stabilized. For the present early development stage, the accuracy and dispersion characteristics of Figs. 11 through 13 are considered to be reasonable. The results also indicate that further development could provide significant improvements.

3. High Penetration Capability

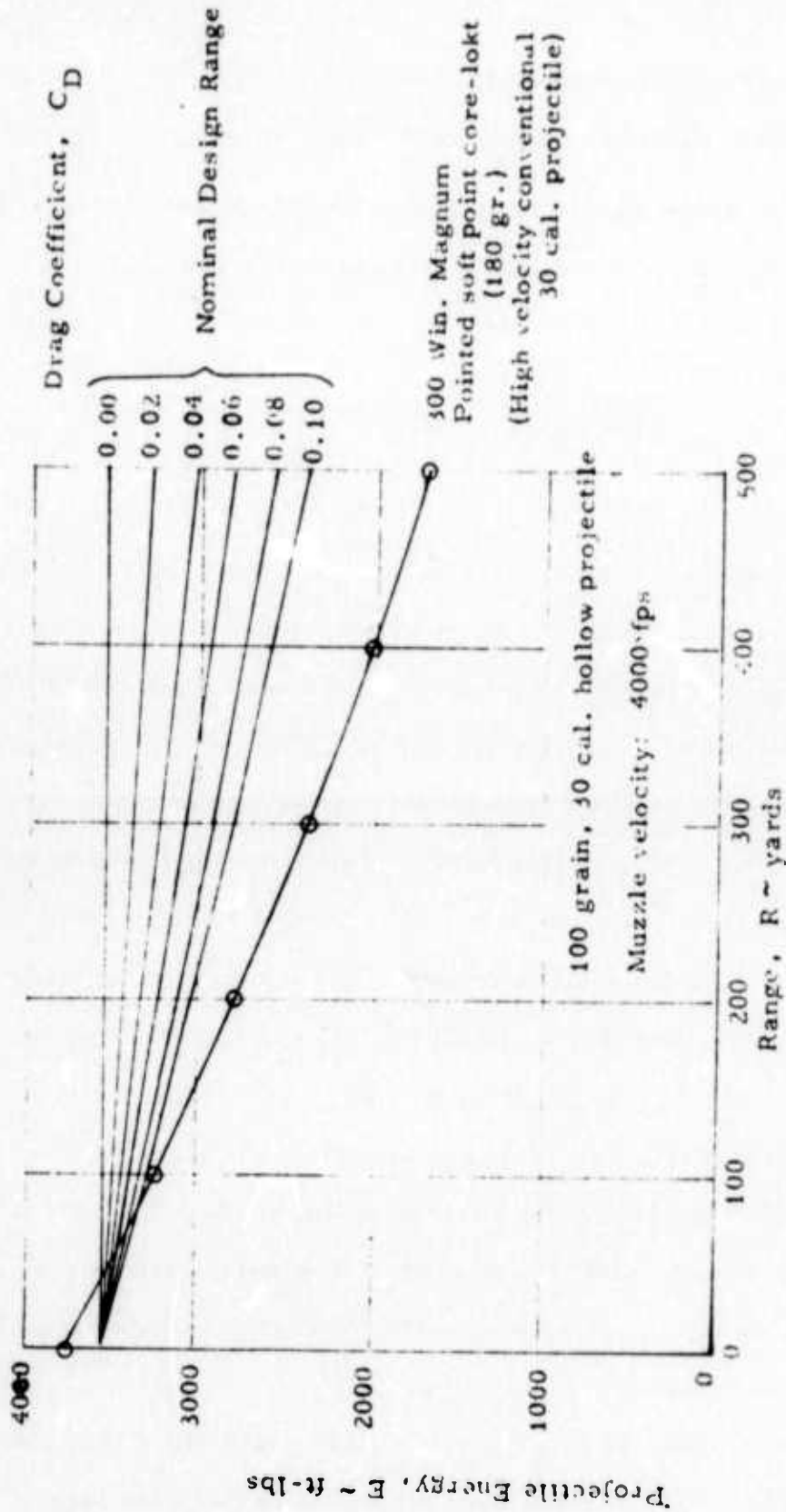
Hollow projectiles possess high penetration capability due to delivery of higher kinetic energy at higher speed. High energy at the target results directly from low drag (Fig. 2) corresponding to low energy dissipation. High speeds are delivered by having lighter projectile weights and heavier propellant weights in conjunction with low drag.

a. Kinetic Energy Delivery

The analytically estimated performance or energy decay characteristics of an example 7.62 mm hollow projectile are presented in Fig. 14 as a parametric function of drag coefficient C_D . The example hollow projectile has the following characteristics:

Diameter: 7.62 mm [30-caliber]

Length: 2.50 inches



ENERGY DECAY CHARACTERISTICS
Comparison of Hollow and Standard Projectiles

Fig. 14

Mass: 100 grains [1/70 lbs]

Muzzle Velocity: 4000 ft/sec [M ≈ 3.6]

Next, refer to the line separating the "starting" and "decelerating" regions of Fig. 5. To just accomplish starting at an initial (muzzle) Mach number of M ≈ 3.6, it follows that

$$\frac{\text{throat area}}{\text{inlet area}}, \frac{A_t}{A_i} \approx 0.685$$

For a projectile of length $l = 2.50$ inches at a Mach number of $M \approx 3.6$, it is seen from Fig. 4 that $C_D \approx 0.062$. However, as the Mach number decreases, the drag coefficient increases. To estimate an appropriate nominal value for C_D , the present illustrative example is focused on target distances within 500 yards. Then, at 500 yards, using a nominal value of $C_D \approx 0.07$, it is found [from Eq. (11) of Ref. 4] that $V \approx 3500$ ft/sec. The corresponding Mach number, based on sea level standard day conditions is $M \approx 3500/1120 \approx 3.1$. Thus, for $C_D \approx 0.07$, the projectile velocity decays from $M \approx 3.6$ to $M \approx 3.1$ in traversing a range of 500 yards. From Fig. 4, the drag coefficient corresponding to $M \approx 3.1$ is $C_D \approx 0.078$. Thus, since $0.062 < 0.070 < 0.078$, it is clear that $C_D \approx 0.07$ is a reasonable nominal value.

As shown on Fig. 14 a curve corresponding to $C_D = 0.07$ would be within the selected nominal design range. The parametric curves for differing values of C_D clearly show the importance of achieving the lowest possible value for C_D .

Also shown on Fig. 14 is a curve for a 180 grain 300 Winchester Magnum projectile. This is a standard projectile having very high performance. It has a muzzle velocity of 3070 ft/sec corresponding to

a muzzle energy of 3770 ft-lbs. This muzzle energy slightly exceeds the muzzle energy of 3550 ft-lbs for the example hollow projectile.

However, the hollow projectile still shows much greater energy delivery at the target. For example, at 500 yards and a nominal $C_D \approx 0.07$ the hollow projectile has an energy of $E_h \approx 2700$ ft-lbs while the conventional 300 Winchester Magnum has an energy of $E_c = 1700$ ft-lbs. The percentage increase in energy at the target is then

$$\frac{E_h - E_c}{E_c} = \frac{2700 - 1700}{1700} \approx 60\%$$

This indicates that 60% more energy is delivered to the target by the example hollow projectile. The comparison is somewhat conservative since the conventional projectile had slightly more initial energy. Further, the selected example hollow projectile is not necessarily the optimum configuration.

The delivery of higher kinetic energy to the target of course represents potential for greater damage and a greater penetration depth.

b. Impact/Penetration Analysis

A formula has been developed for the penetration depth P of a projectile into a semi-infinite medium. It is based upon an extension of Awerbach's approach to the penetration of thin plates (Ref. 11). The formula is

$$\frac{P}{I} = \frac{1}{k} \left(\frac{\rho_p}{\rho_t} \right) \left[\left\{ \frac{(K_s + 2) \rho_t V^2}{k_1 \rho_p C_t^2} + 1 \right\}^{\frac{1}{K_s + 2}} - 1 \right] \quad (13)$$

where:

m_p = mass of the projectile

ρ_t = density of the target

A = projected area of missile nose on the target

V_p = projectile velocity

ρ_p = density of projectile

C_t = acoustic velocity of target material

K_s = constant related to shape of projectile's nose

k, k_1 = empirical constants

The constant K_s is equal to unity for a cylindrical projectile, and can, in principle, be calculated for other shapes. The constant k_1 is related to the maximum strength of the target; it is hoped to establish a rational basis for its selection, however it must presently be treated as an empirical constant. The same is true for k .

It is customary, in presenting the results of impact tests with spherical projectiles, to plot P/d versus $(\rho_p/\rho_t)(V_p/C_t)$ where d is the diameter of the projectile. Summers and Charters (Ref. 12) have presented an empirical formula for the penetration depth for this case which is based upon the assumption that the projectile energy is deposited uniformly in a hemispherical volume of the target which becomes the crater. Their formula is

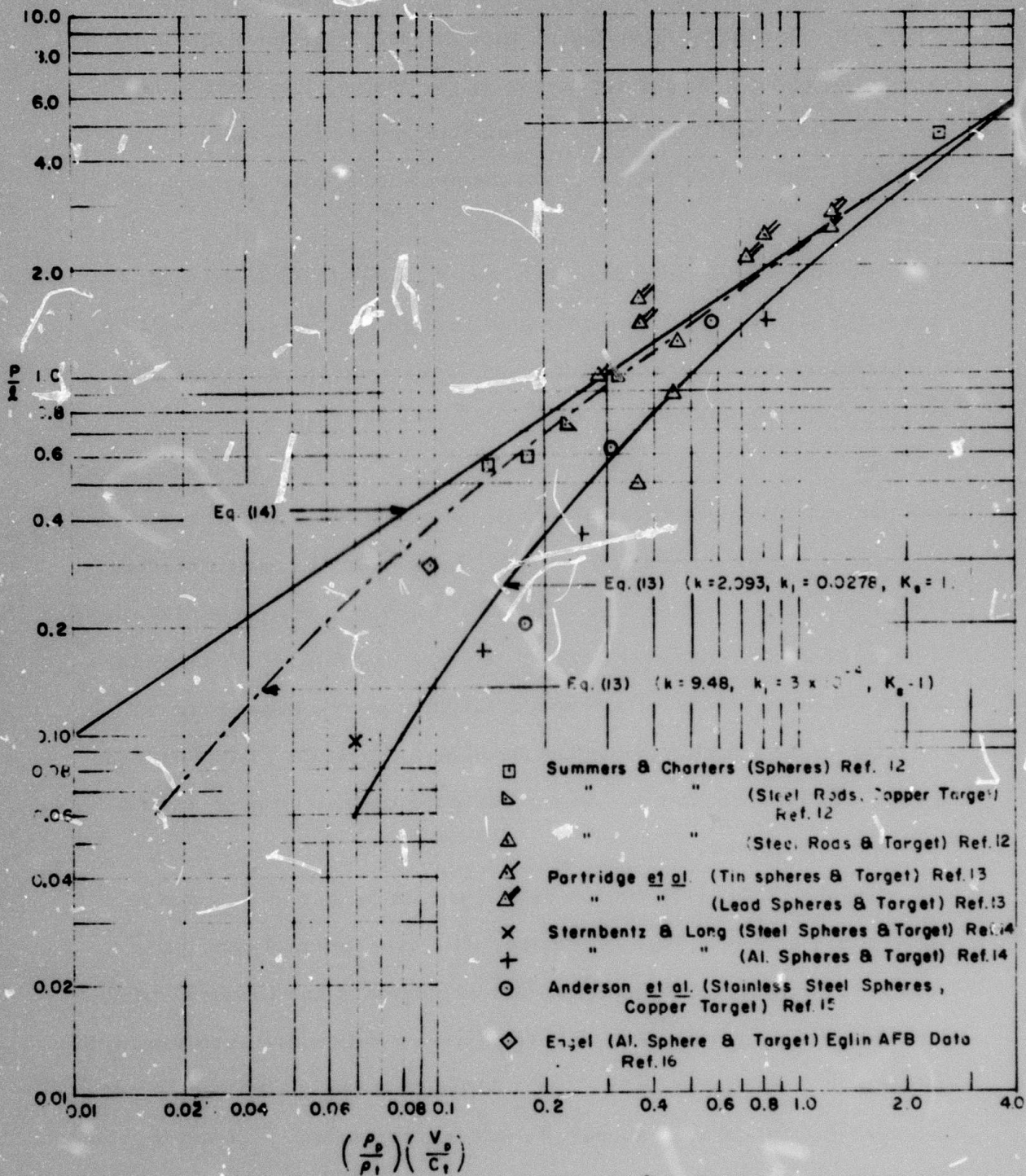
$$P/d = 2.28(\rho_p/\rho_t)^{2/3}(V_p/C_t)^{2/3} \quad (14)$$

They show data for a variety of projectile and target materials which appear to confirm this relation for a range of the ordinate parameter $(\rho_p/\rho_t)(V_p/C_t)$ from about 0.13 to about 3. However, data from

other sources departs from the relation for values of the ordinate parameter below about 1.0, and appears to follow another law. Some data from Summers and Charters for cylindrical projectiles, when plotted as (P/l) , where l is the length of the projectile, also appear to follow the latter law.

By appropriate selection of k and k_1 , Eq. (13) can be made to approach the relation of Summers and Charters for large values of the ordinate parameter, and to conform to the experimental data which departs from their formula at low ordinate values. By a different choice of k and k_1 , Eq. (13) can be made to conform to all of the experimental data presented by Summers and Charters for spheres, and to approach a different law at lower ordinate values. However, the data from other sources would not then be fitted as well. From this and from discussion of impact theory in the literature, it is clear that the impact process involves factors characteristic of the target material which may not be reflected in the simpler empirical formulas. Hopefully, some of these factors will be accounted for once a basis for the selection of k and k_1 has been determined.

Graphs of Eq. (13) for two sets of values of k and k_1 , and of Eq. (14) are shown in Fig. 15 together with experimental data taken from several sources. (Since the data of Summers and Charters fit the line labeled Eq. (14) so well, only the extreme points are shown to avoid clutter.) K_s was taken to be unity. Although there is some scatter in the experimental data, it appears to fall into two groups, an upper group and a lower group. For high values of the ordinate parameter, these two groups converge. It is seen that the upper group is fitted equally well by Eq. (14) and Eq. (13) for one choice of k and k_1 , while the



CORRELATION OF PROJECTILE PENETRATION DATA AND THEORIES

Fig. 15

lower group is fitted best by Eq. (13) with the other choice of k and k_1 .

To the extent that this Figure can be taken as a verification of the general form of Eq. (13), certain conclusions may be drawn regarding the expected performance of the hollow bullet relative to that of a conventional bullet. As an example, a comparison of the penetration of a solid steel cylinder and a hollow steel cylinder impinging on a steel target are given in Fig. 16 corresponding to the two selected sets of values of k and k_1 . The impact energies of the two bullets are assumed to be equal.

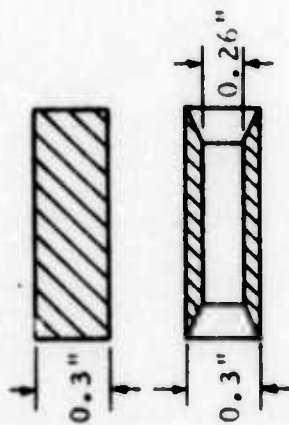
The ratio of the masses of the two bullets (solid/hollow) was four, so, with the same impact energy, the velocity ratio (solid/hollow) was one half. In an actual case, the reduced drag of the hollow bullet should allow it to arrive at the target with higher energy provided that the energy going into the sabot can be kept small.

From Fig. 16 it is seen that the theory indicates that the hollow projectile will have approximately twice the penetration depth for the same energy at the target. This example illustrates the very high penetration potential of hollow projectiles.

c. Penetration Testing

Firing tests confirm that the hollow projectile can provide greatly improved armor penetration characteristics. A series of hollow projectiles were fired into a standard helmet located 50 feet from the muzzle. A set of ballistic screens located within about 16 feet from the muzzle indicated that high muzzle velocities of approximately 5500 fps were attained.

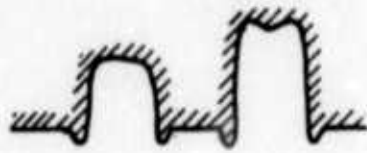
Steel Projectile



Solid (heavy, slow)

Hollow (light, fast)

Steel Target



Configuration	Length (in.)	O.D. (in.)	I.D. (in.)	Mass (grains)	Vel. (fps)	Energy (ft-lbs)	Penetration (in.)
Solid	1	0.3	--	140	3000	2795	0.630
Hollow	1	0.3	0.26	35	6000	2795	1.059

$$k = 9.48 \quad k = 2.093$$

$$k_1 = 3 \times 10^{-4} \quad k_1 = 0.0278$$

IMPROVED PENETRATION

Hollow vs. Solid Cylindrical Projectile
(Equal Impact Energy)

Fig. 16

The high-speed hollow projectiles "punched" clean holes in both the entering and exiting surfaces of the helmet. A round metal core was cut from the helmet surfaces and the metal around the hole was essentially not dented or deformed. In contradistinction to these clean holes, standard pointed-nose projectiles deform the surface while leaving ragged holes. These results are illustrated in Fig. 17.

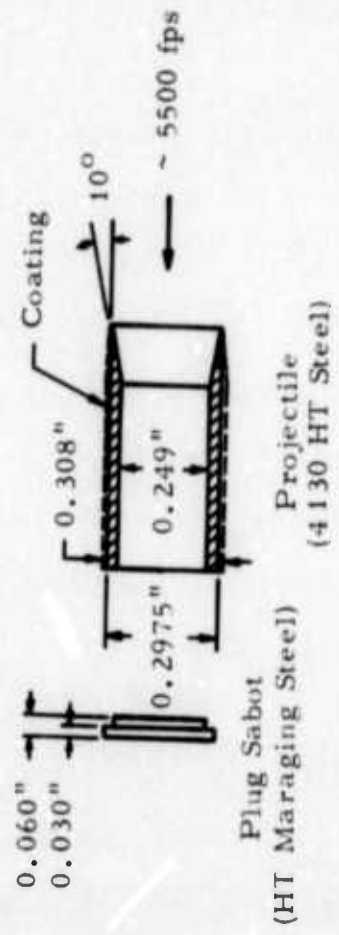
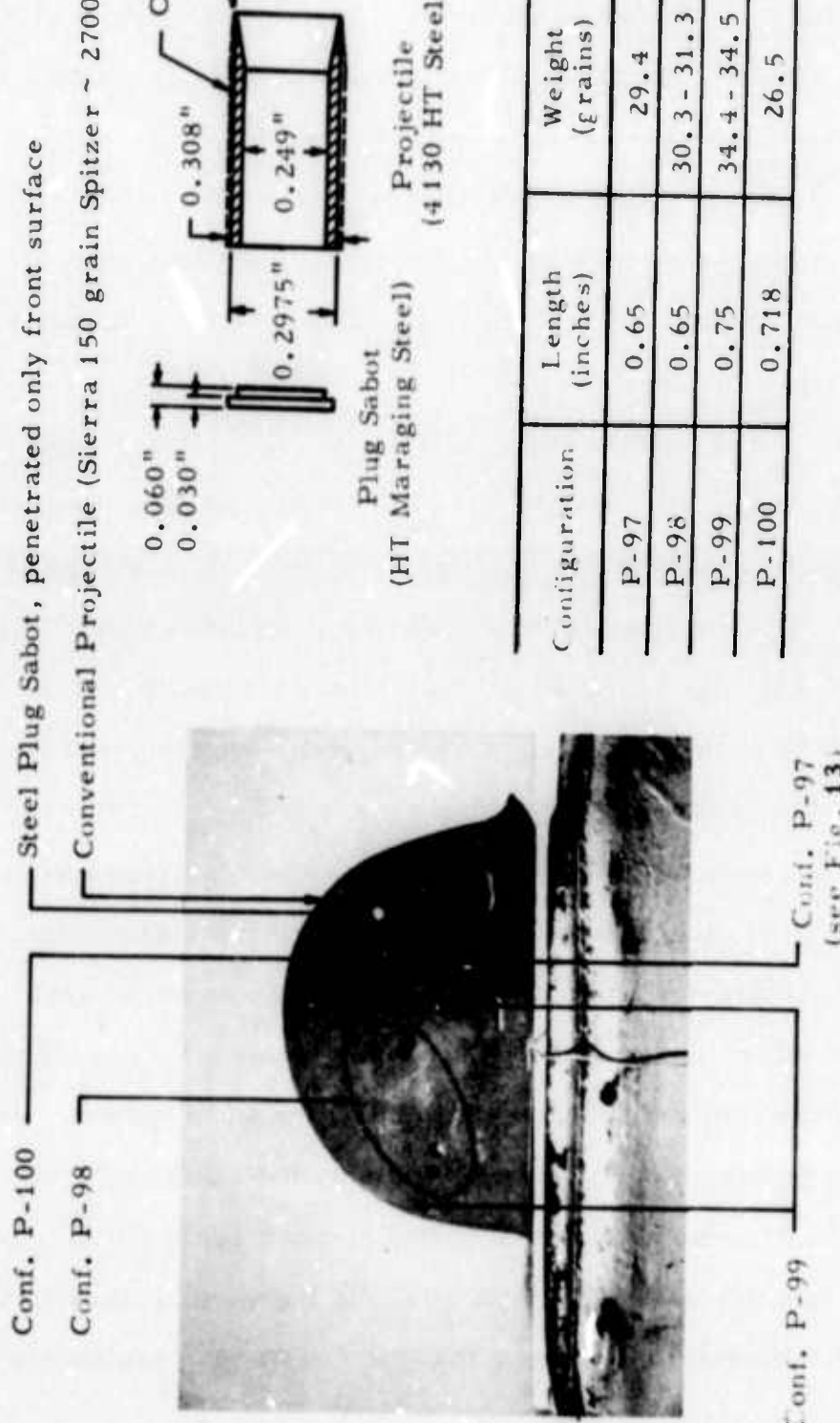
Thus, the hollow projectile does not expend energy in deforming the surrounding metal surfaces and from this viewpoint more of its energy is used in penetration. This is indicative of potential for greater penetration.

As noted on Fig. 17, four (4) hollow projectile configurations (P-97, P-98, P-99, and P-100) were fired. All these projectiles penetrated both surfaces. Except for P-99 at the left edge of the helmet, both entry and exit holes were clean as described above. The entry holes at the edge of the helmet were clean but oblong and the exit hole from P-99 at the far left edge was ragged, indicating that the projectile had tumbled due to its very oblique entry.

As shown on Fig. 17, thin heat treated Maraging steel plug sabots were used to launch the projectiles. One of these sabots hit the helmet and penetrated one surface. Such simple sabots are suitable for the present effort directed toward assessing projectile characteristics.

However, for many applications more advanced sabot systems must be employed. For example, non-lethal sabots are required for many small arms applications. For aircraft applications, "consumable" sabots are desirable to obviate possible ingestion of sabots in engines.

Additionally, it is clear that the simple plug sabot does not provide



Configuration	Length (inches)	Weight (grains)	Coating Material
P-97	0.65	29.4	Copper
P-98	0.65	30.3 - 31.3	Copper
P-99	0.75	34.4 - 34.5	Copper
P-100	0.718	26.5	Polypropylene

HVI MET PENETRATION TESTS
Fig. 17

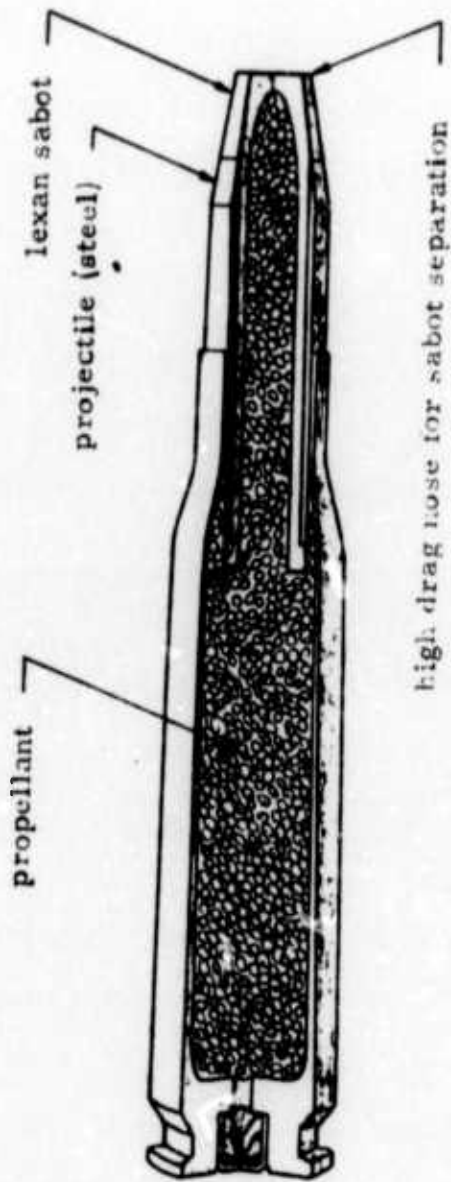
the highest possible performance. It does not permit the hollow space inside the projectile to be utilized for propellant and thereby penalizes muzzle velocity and energy.

In fact, the muzzle energy of the hollow projectiles in Fig. 17 is generally slightly below the reference conventional projectile due to the use of these simple non-optimum sabots. However, penetration is greatly improved even on the basis of equal energy as indicated in Figs. 16 and 17. For down range targets, the hollow projectile will possess greater energy (due to low drag) than conventional projectiles and thereby exhibit even greater relative penetration capability (e. g. , Fig. 14).

These improved penetration capabilities can be fully exploited via development of advanced sabot systems. After such sabot systems are developed, additional impact/penetration testing would be justified to completely demonstrate the penetration performance of a practical hollow projectile ammunition system.

B. OPERATIONAL ADVANTAGES

A successful hollow projectile ammunition system must be operationally feasible in addition to providing high performance as documented above. A key factor involves development of compact systems featuring sabots which allow the hollow interior space of the projectile to be packed with propellant. An example projected retrofit design (i. e. , useable in existing weapons) is shown in Fig. 18.



- Low Weight and Drag
- Simple and Inexpensive
- Low Recoil
- High Speed and Impact Energy
- High Effective Range and Flat Trajectory
- Superior Target Penetration

EXAMPLE HIGH PERFORMANCE COMPACT RETROFIT HOLLOW PROJECTILE SYSTEM
FOR 7.62 mm WEAPONS

Fig. 18

1. Compactness/Sabot Development

Although the present effort concentrated mainly on simple non-compact sabots, some sabot development activity focused on ultimately evolving compact systems was initiated. Along with compactness, it is necessary to consider factors such as (1) protection of sharp surfaces during loading, and (2) design features to insure non-lethality of the sabot (see Fig. 18).

a. Developmental Results

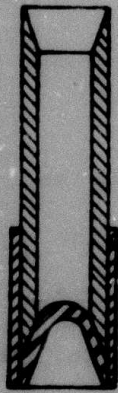
A simple non-compact plug sabot launching system was developed as a "workhorse" sabot to allow evaluation of the basic hollow projectile under firing range conditions. During the course of this investigation four basic sabot configurations (Fig. 19) were investigated.

- Internal Cup Sabot -- shaped steel inner cup with gilding metal outer sleeves
- External Cup Sabot -- flat steel base with lexan external cup
- Plug Type Sabot -- simple base plug of lexan or steel
- Forward Sabot -- lexan forward cup external to projectile

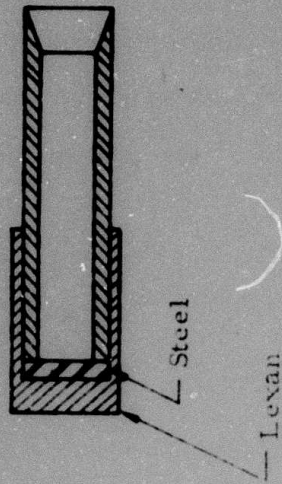
The forward sabot is the only configuration of those above which qualifies as a compact system.

Varying degrees of success were achieved with these configurations. Some typical results and problems encountered with the cup sabot arrangement are illustrated on Fig. 20. It was generally difficult to make the inner cups separate from the projectile. The thin outer sleeves were to unfold and create high drag to help separation. They successfully unfolded but tore loose so that they did not exert the desired high drag. Further developmental work would probably have solved these problems.

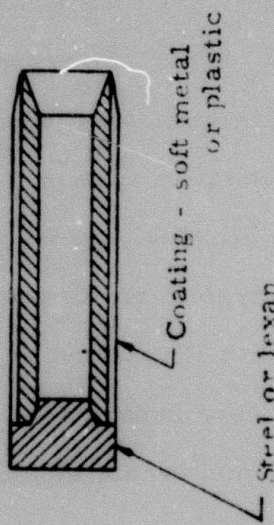
Internal Cup Sabot



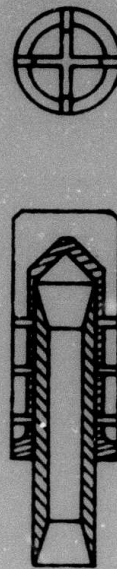
External Cup Sabot



Plug Type Sabot



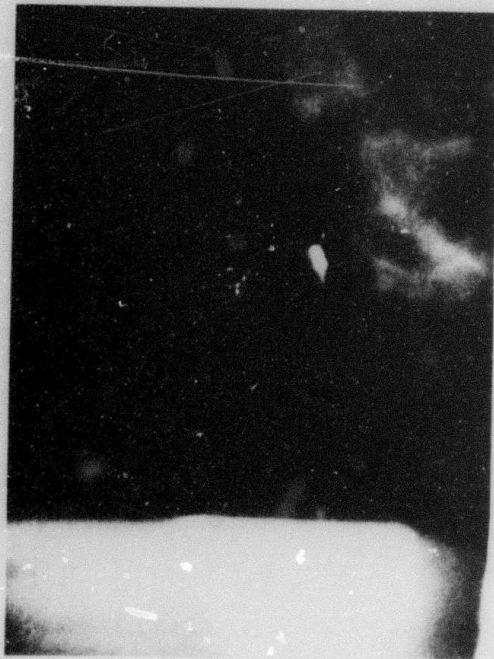
Forward Sabot



EXPERIMENTALLY INVESTIGATED SABOT CONFIGURATIONS

Fig. 19

INTERNAL CUP



- ←
- Outer Gilding Metal Sleeves Pulled Open But Tore Loose
 - Inner Cup Did Not Separate From Projectile

EXTERNAL CUP



- ←
- Outer Lexan Sleeves Pulled Open But Tore Loose
 - Sabot Separated Completely From Projectile

CUP SABOT SEPARATION PHOTOGRAPHS

Fig. 20

However, the plug sabot provided the greatest reliability and assurance that the proper spin rate was being imparted to the projectiles. Further, it was lighter and easier to manufacture. It was thus selected as the "workhorse" for demonstrating the basic performance potential of the hollow projectile.

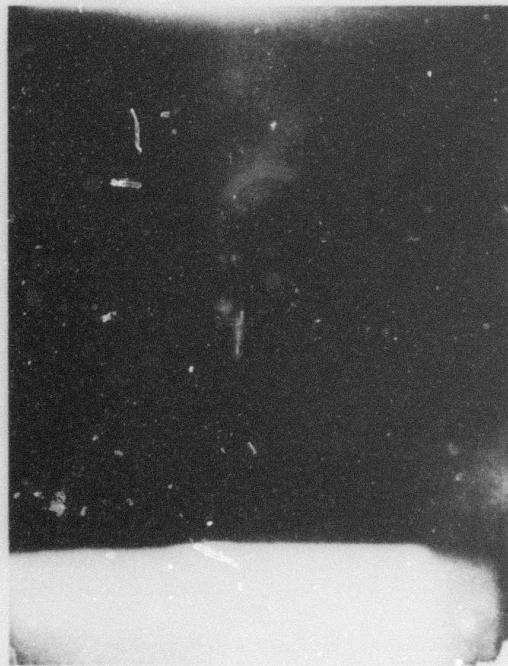
The selected plug sabot was developed to the point where it consistently separates cleanly from the projectile. This was photographically verified during firing range tests (e.g., Fig. 21). For hand loading simplicity, the thinner maraging steel plug (Fig. 17) was employed on the latest test runs.

The selected "workhorse" sabots were employed to launch projectiles weighing from 15 to 40 grains at speeds between 3500 and 6000 ft/sec. A range of DuPont propellants including IMR 3031, IMR 4198 and IMR 4227 was employed. Thus, sufficiently high speeds have been achieved to permit swallowing of the bow shock. When the bow shock is swallowed efficient supersonic flow is established as determined via wind tunnel testing (Fig. 5).

Only a few preliminary tests were made on the forward sabot. Lexan was used for simplicity although calculations indicated higher strength materials would be more optimal (i.e., thinner and lighter). Partial success was achieved in fragmenting the head portion of the sabot at the muzzle. But completely clean separation was not achieved. These tests are however promising with regard to development of such compact forward sabot configurations.

The forward sabot engages the rifling and transmits spin to the projectile. Other compact arrangements such as that illustrated in the

LEXAN PLUG



NOTES:

- (1) Clean Separation From Coated Projectiles
- (2) Projectile Located 15" From Muzzle

MARAGING STEEL PLUG



PLUG SABOT SEPARATION PHOTOGRAPHS

Fig. 21

projected arrangement of Fig. 18 would require transmission of spin directly to the projectile via a thin soft metal or plastic coating.

Development of soft metal and plastic coatings was undertaken for use with the simple "workhorse" plug sabot system (Fig. 19). This development work is directly applicable to projected systems like that of Fig. 18.

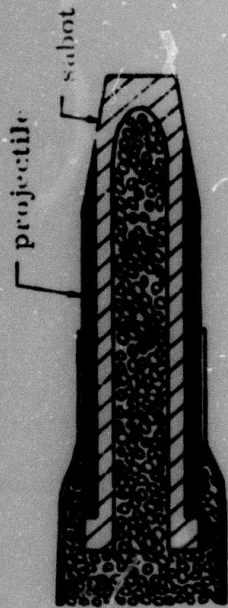
The results of this activity indicate that a polypropylene coating applied via techniques developed at Hercules provides a strong coating that successfully imparts spin. Plating of soft metals such as copper and gilding metal also provide successful coatings. It was found that coating and plating techniques must be carefully monitored to avoid coatings that would shear off. The type of coating could also have some aerodynamic effects as discussed previously (in connection with Figs. 11 through 13).

b. Projected Systems

The extensive sabot development activity already accomplished indicates that there are three primary compact systems. These projected systems are summarized in Fig. 22 where major characteristics of each system are tabulated.

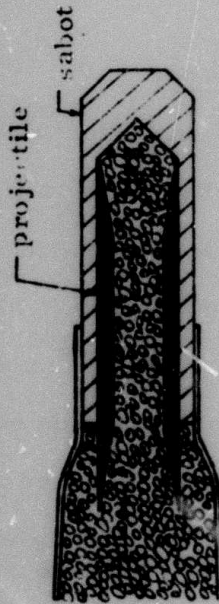
(1) Internal Forward Sabot

The first configuration (also shown in Fig. 18) is termed an "internal forward sabot" arrangement. The sabot is shaped like a thimble and the projectile fits over this thimble sabot like an outer sleeve. The forward section of the thimble protrudes ahead of the



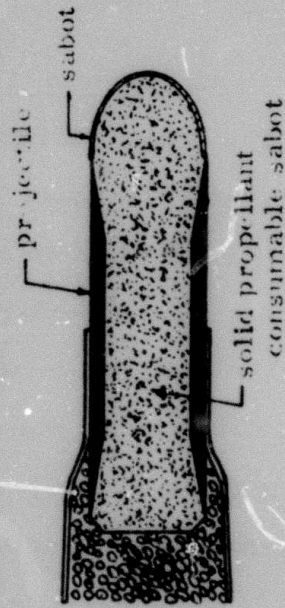
a. Internal Forward Sabot

- Permits use of maximum diameter projectile
- Allows conventional chambering
- Spin imparted via soft coating on projectile
- More readily applicable to external bevel than internal bevel configuration



b. External Forward Sabot

- Readily applicable to internal bevel configurations
- Eliminates requirement for projectile coating
- Spin imparted via sabot
- Allows conventional chambering
- Necessitates reduced projectile diameter



c. Consumable Sabot

- Permits use of maximum diameter projectile
- Consumable sabot provides thrust and greater muzzle velocity
- Thin forward shell allows conventional chambering
- Spin imparted via soft coating on projectile
- Requires development of consumable sabot materials along with bonding techniques

PROJECTED COMPACT HOLLOW PROJECTILE SYSTEMS

Fig. 22

sleeve or projectile and is shaped to allow chambering of the projectile/ cartridge assembly when fired from conventional weapons such as the M14 rifle or M60 machine gun.

When the "internal forward sabot" arrangement is fired, gas pressures act on the inner surface of the sabot to drive it down the barrel. The projectile is engaged to the sabot by a step in the rear part of the sabot and by friction between the mating projectile and sabot surfaces. Thus, the projectile is also driven down the barrel.

A soft coating of plastic or metal on the outer surface of the projectile engages the rifling in the barrel to impart the required spin. When the projectile/sabot assembly leaves the muzzle, dynamic pressure generated by forward speed acts on the larger projected frontal area of the inner sabot and forces it rearwards out of the projectile. When complete separation is accomplished, the projectile proceeds at high speed while the light sabot rapidly decelerates (i.e., the sabot will be non-lethal).

(2) External Forward Sabot

The second configuration is an "external forward sabot" arrangement. Here, the sabot is again shaped like a thimble. But the projectile now fits inside the thimble. The forward section of the thimble is again shaped to allow chambering in conventional 7.62 mm weapons.

The "external forward sabot" is driven down the barrel upon firing. The gas pressure acting on the inside of the thin wall projectile tends to cause the projectile to expand outward and enhance the frictional bond between the sabot and projectile. In this way, the projectile is pulled down the barrel by the forward sabot. Also, the outer sabot

engages the rifling and transmits spin to the projectile via the same frictional bond.

The forward section of the sabot is designed to remain intact as long as it is supported by the walls of the rifling barrel. Thus, when it protrudes from the muzzle, the support vanishes and it is fragmented. The projectile is then free to proceed at high speed.

(3) Consumable Sabot

The third retrofit configuration is characterized as a "consumable sabot" arrangement. A solid propellant consumable sabot is bonded to the inside of the solid projectile. Upon firing, this consumable sabot must remain intact and burn from its aft base. As it burns it provides a thrust and is designed to be completely consumed when the projectile is at the muzzle. The thin forward shell will then be fragmented (by muzzle gas pressure) and the hollow projectile will be launched.

This system has potential for high performance due to the "travelling charge effect." This effect is of particular value for high speed firings and is highly compatible with hollow projectiles where high speed launchings are desirable. Lethality and ingestion (aircraft applications) problems will also be circumvented.

2. Lightweight Ammunition System

Compared to conventional projectiles of the same weight and caliber, thin-walled hollow projectiles are inherently lightweight. They must therefore be fired at higher velocities to achieve the same muzzle energy. At the same muzzle energy, they will have lesser recoil, which enhances handling and improves accuracy.

When the constraint of using conventional existing weapons and cartridge cases is removed, even more compact and lightweight ammunition systems will result. In a basic sense, the hollow projectile can serve the same role as the cartridge. The projectile can then be made longer while minimizing or eliminating the cartridge case.

This will of course necessitate a modified weapon. Existing 7.62 mm weapons use necked down chambers and cartridge cases whereas the compact arrangement (minimal cartridge case) must use a straight chamber of essentially the same diameter as the barrel bore.

The three basic compact arrangements shown in Fig. 20 can be configured to essentially eliminate the cartridge case. Both the internal and external forward sabot arrangements could be made longer with a very short cartridge case of essentially the same outer diameter mounted on the aft end. The consumable sabot arrangement could also be elongated and the case could be entirely eliminated if ignition techniques similar to those employed with caseless ammunition were employed.

Lightweight provides obvious operational advantages. Basically a greater quantity of ammunition can be carried to enhance firepower. The higher speeds associated with lightweight ammunition result in flat trajectories, greater penetration and short travel times to enhance accuracy and kill probability.

3. Inexpensive Manufacture/Design Simplicity

Hollow projectiles are inexpensive and simple to manufacture. The basic projectile is a thin-walled cylindrical steel tube with a soft metal or plastic coating. The ends of the tube are beveled to reduce drag. It is readily envisaged that this simplicity will lead to low cost

automated machine fabrication techniques.

Lightweight, compact sabot systems as shown on Fig. 22 also appear to be fundamentally simple and inexpensive. Further developmental testing is required to fully assess these systems. However, sabot investigations during this program are very promising with regard to successful development.

Thus, the present investigation demonstrates that hollow projectiles can provide improved performance and operational advantages at a low cost.

III. CONCLUSIONS AND RECOMMENDATIONS

The central conclusion of the present investigation is that high performance hollow projectile systems are basically feasible. Continued effort is required to exploit the demonstrated order of magnitude potential improvement via investigation of practical compact ammunition systems.

This further activity will involve detailed ramifications and trade-offs within the fundamental framework established in this report. The manifold interrelations include:

- Aerodynamic projectile shape optimization in relation to sabot system design for (1) clean separations and (2) high accuracy with low dispersion.
- Projectile weight and length/diameter ratio compatible with desired spin rate and muzzle velocities to maximize target penetration at selected distances.

Basic steps should encompass: (1) aerodynamic/design analysis, (2) wind tunnel testing, and (3) comprehensive firing range tests. Major effort must be directed toward developing a practical compact sabot system. Wind tunnel tests are required to determine low drag projectile configurations that are compatible with the selected compact sabot system. Firing range tests are necessary to delineate design characteristics leading to accuracy, low dispersion, and high penetration.

The further activity described above is warranted by the results of the present study. Hence, such an effort is recommended.

Preceding page blank

REFERENCES

1. Wu, J. J.: 'Performance Characteristics of a 'Silent' Projectile,' VRC Working Paper No. 208, September 1970.
2. Schlichting: Boundary Layer Theory. 4th Edition, McGraw-Hill, 1960.
3. Liepmann, H. W., and Goddard, F. E.: 'Note on the Mach Number Effect Upon the Skin Friction of a Rough Surface,' Jour. Aero. Sci., 24, 784, 1957.
4. Sargent, E. R.: "High Performance Projectile, Quarterly Progress Report No. 1," ARPA Order No. 1575, SASA Contract No. DAAD05-72-C-0296, Vehicle Research Corporation report, 31 August 1972.
5. Sargent, E. R.: "High Performance Projectile, Quarterly Progress Report No. 2," ARPA Order No. 1575, SASA Contract No. DAAD05-72-C-0296, Vehicle Research Corporation report, 30 November 1972.
6. Hill, Philip G., and Peterson, Carl R.: Mechanics and Thermodynamics of Propulsion, Addison-Wesley Publishing Company, Inc., Reading, Massachusetts, 1965.
7. Oswatitsch, K.: "Pressure Recovery for Missiles with Reaction Propulsion at High Supersonic Speeds (The Efficiency of Shock Diffusers)," NACA TM 1140, June 1947.
8. Kantrowitz, Arthur, and Donaldson, Coleman duP.: "Preliminary Investigation of Supersonic Diffusers," NACA Wartime Report No. I-713 (ARC No. L5D20), May 1945.
9. Sargent, E. R.: "High Performance Projectile, Quarterly Progress Report No. 3," ARPA Order No. 1575, SASA Contract No. DAAD05-72-C-0296, Vehicle Research Corporation report, 28 February 1973.
10. Liepmann, H. W., and Roshko, A.: Elements of Gas Dynamics, John Wiley and Sons, Inc., New York, 1957.
11. Awerbach, J.: "Mechanics Approach to Projectile Penetration," USAF OSR Contract F 61052-69-C-0042 Scientific Report No. 6, May 1970 (AD 716 001).
12. Summers, J. L., and Charters, A. C.: 'High Speed Impact of Metal Projectiles in Targets of Various Materials,' Proc. Symp. Hypervelocity Impact, 3rd, Armour Research Foundation, Chicago, Ill. (Feb. 1959).

13. Partridge, W. S., Vanfleet, H. B., and Whited, C. R.: "Crater Formation in Metallic Targets," J. Appl. Phys., V. 29, No. 9, pp. 1332-1336, Sept. 1958.
14. Sternbentz, W. H., and Long, L. L.: "Meteoroid Effects on Nuclear Rocket Space Vehicle Mission Success," Sixth Symposium on Hypervelocity Impact, V. III, Aug. 1963.
15. Anderson, C. D., Doran, D. G., Hempy, F. S., and Kells, M. C.: "Cratering on High Velocity Microparticles," Proc. Symp. Hypervelocity Impact, 3rd, Armour Research Foundation, Chicago, Ill. (Feb. 1959).
16. Engel, O. G.: "Hypervelocity Cratering Data and a Crater-Depth Model for the Regime of Partial Fluidity," Proc. Symp. Hypervelocity Impact, 6th, Cleveland, Ohio, April 30, May 1, 2, 1963.

APPENDIX

EXPERIMENTAL FACILITIES AND TEST PROCEDURES

The experimental results contained in this report were obtained in wind tunnel and firing range facilities set up by VRC. These facilities and associated operating procedures are described in this Appendix.

A. SUPERSONIC WIND TUNNEL

1. Facility Description

A 2" X 2" supersonic wind tunnel was employed for investigating the aerodynamic characteristics of the hollow projectile. The wind tunnel is installed on the VRC premises. The compressor and storage tank are located outside of a building housing the test section and control panel. This minimizes noise and facilitates tunnel operation and data taking. The test section arrangement is shown in Fig. A-1.

The wind tunnel characteristics are as follows:

TYPE: Supersonic Blowdown

MANUFACTURER: Kenney Engineering
Monrovia, California

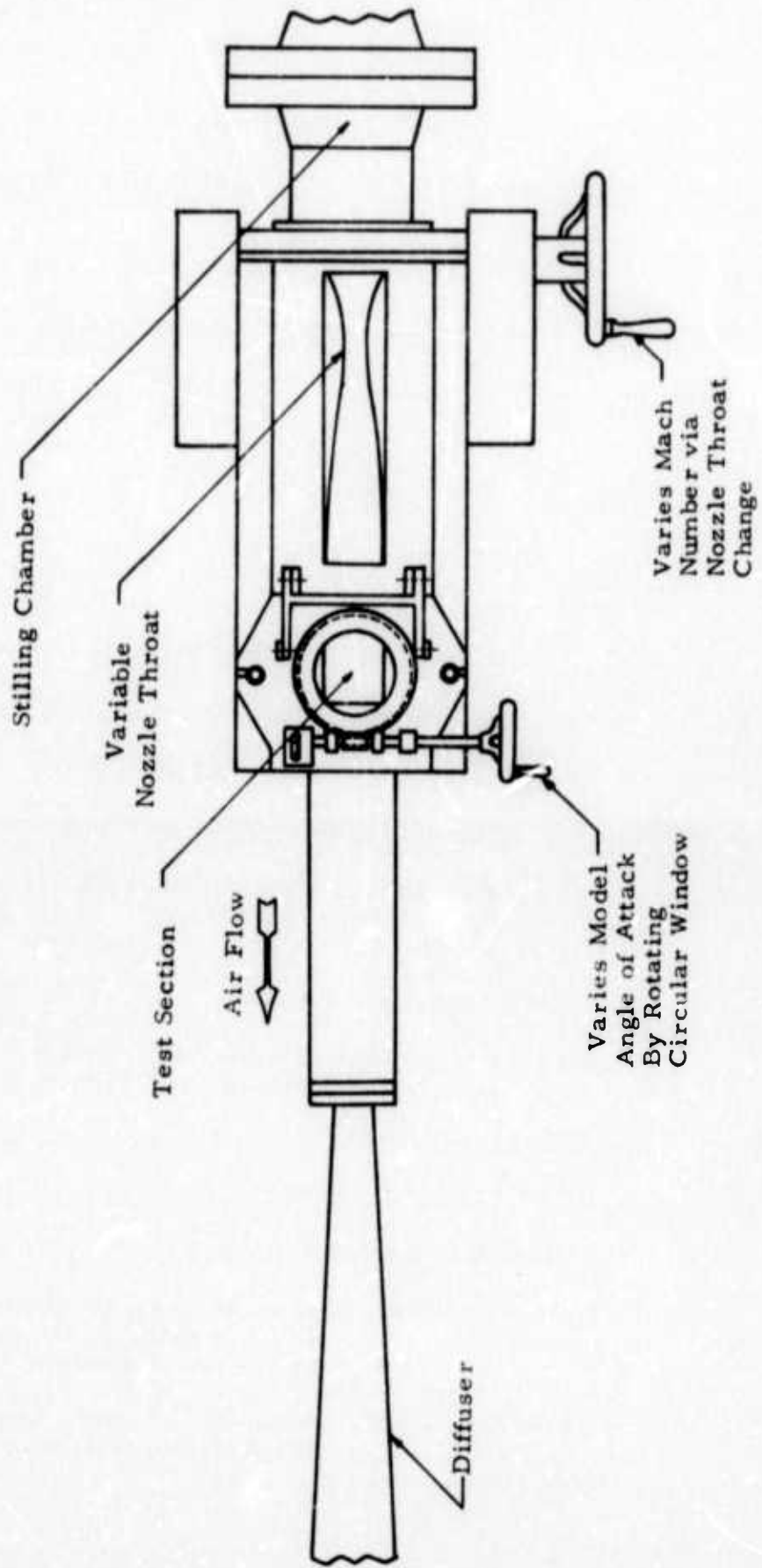
MODEL NO: 1024

TEST SECTION: 2" X 2"

MACH NO. RANGE: 0 - 4.5

COMPRESSOR: Two-stage Gardner-Denver Model No.
ADR-1014 rated at 250 psig and driven by a
a 15 HP electric motor

STORAGE TANK: Volume = 80 cubic feet
Maximum operating pressure = 265 psi



WIND TUNNEL TEST ARRANGEMENT
 Kenney Engineering 2" X 2" Supersonic Wind Tunnel Model 1024

Fig. A-1

The Mach number is varied by changing the wall contour and throat opening upstream of the test section. This Mach number variation can be accomplished while the wind tunnel is operating. The upper and lower walls of the wind tunnel are made of flexible steel which permits the required contour changes. These changes are accomplished via a manual crank/gear mechanism (see Fig. A-1). The side walls are made of glass so that Schlieren techniques can be employed.

The test section is accessible through a circular 4-3/8 inch diameter port. The circular wall section which fits in the port is comprised of a steel outer ring holding a circular glass inner section. This wall section additionally contains provisions for mounting models and/or probes for pressure instrumentation.

The circular wall section is held in a hinged mounting bracket mechanism. This mechanism contains a worm gear arrangement for rotating the circular section. This rotation can be used for longitudinally pitching the model or for varying its vertical location (see Fig. A-1).

The wind tunnel is equipped with a pilot-operated regulator so that the desired test section total pressure can be used. If the minimum setting is used, the longest run duration results. Higher settings increase the test section dynamic pressure as well as the unit Reynolds number. The duration times are of the order of 30 - 45 seconds.

In addition to the regulator valve, the control panel contains pressure gauges to measure the regulator setting, the storage tank pressures, and the test section total pressure (i. e., pressure in stilling chamber downstream of regulator). There is also a gauge to measure the temperature of the gas in the stilling chamber. The start-stop operation of the tunnel is controlled by a solenoid actuated valve.

The tunnel installation also includes a standard concave mirror type Schlieren system. The system employs 3-inch diameter mirrors (focal length of 18 inches) to project the Schlieren picture on a 10 inch by 12 inch screen. A camera can then be employed to photograph the Schlieren picture for a permanent record. The Schlieren apparatus can be moved to provide coverage of any part of the test section. Further, the image size can be varied within limitations of the screen.

For taking force and moment measurements, a three-component balance, Model 1219, is manufactured by Kenney Engineering. This balance is designed especially for the 2" X 2" supersonic wind tunnel (Model 1024) of Fig. A-1.

The balance is circular with a hollow center. It is designed to fit on the outside of the rotating window (Fig. A-1) so that its hollow center will allow visual observation and Schlieren photography through the circular window.

The balance is designed for small interactions (less than 1%) and maximum loads are as follows:

Lift: ± 20 lbs

Drag: ± 20 lbs

Moment: ± 40 in-lbs

2. Test Procedures

Schlieren photography was first used to determine the Mach number for "starting" or shock swallowing. The Mach number was set (variable nozzle throat) for a value higher than the theoretical prediction for starting. A test run was then conducted to confirm the occurrence of proper starting with its associated smooth flow. The Mach setting

was then reduced in stepwise increments and testing repeated until the flow failed to start (signified by presence of bow shock). The minimum Mach number for proper starting was determined by this procedure.

After the projectile starts (bow shock swallowed) its speed can be reduced considerably below the minimum starting speed. At some lower speed, the bow shock will appear to signify that the internal flow has choked. This characteristic behavior was systematically investigated.

The selected test models were started at speeds above the minimum starting speed previously determined. Then the speed was reduced via the crank which varies the nozzle throat (Fig. A-1) until the bow shock (as shown by the Schlieren system) suddenly appeared. The Mach number corresponding to this point is associated with the occurrence of choking accompanied by a large drag increase. It thus denotes the end of high performance flight.

Force and moment measurements were taken by first installing and calibrating (via standard techniques, e.g., Ref. A-1) the three-component balance (Model 1219) previously described. The load cells exhibited linear characteristics with very small interactions within the 1% bound quoted by the manufacturer.

The basic force and moment measuring technique was to vary the pitch angle and measure each of the three components at each selected angle. To reduce data to coefficient form, it was also necessary to record the Mach number and total pressure p_0 .

For example, consider the lift coefficient

$$C_L = \frac{L}{q l} = \frac{L}{\frac{1}{2} \gamma M^2 p l}$$

where

L = lift force determined from calibrated gage

l = model reference length

M = Mach number which is solely a function of the variable
nozzle throat setting

p = static pressure in the test section

γ = ratio of specific heats (= 1.4 for air)

The static pressure p can be determined as a function of the Mach number M and the total pressure p_o as measured in the stilling chamber just upstream of the variable nozzle throat, i. e.

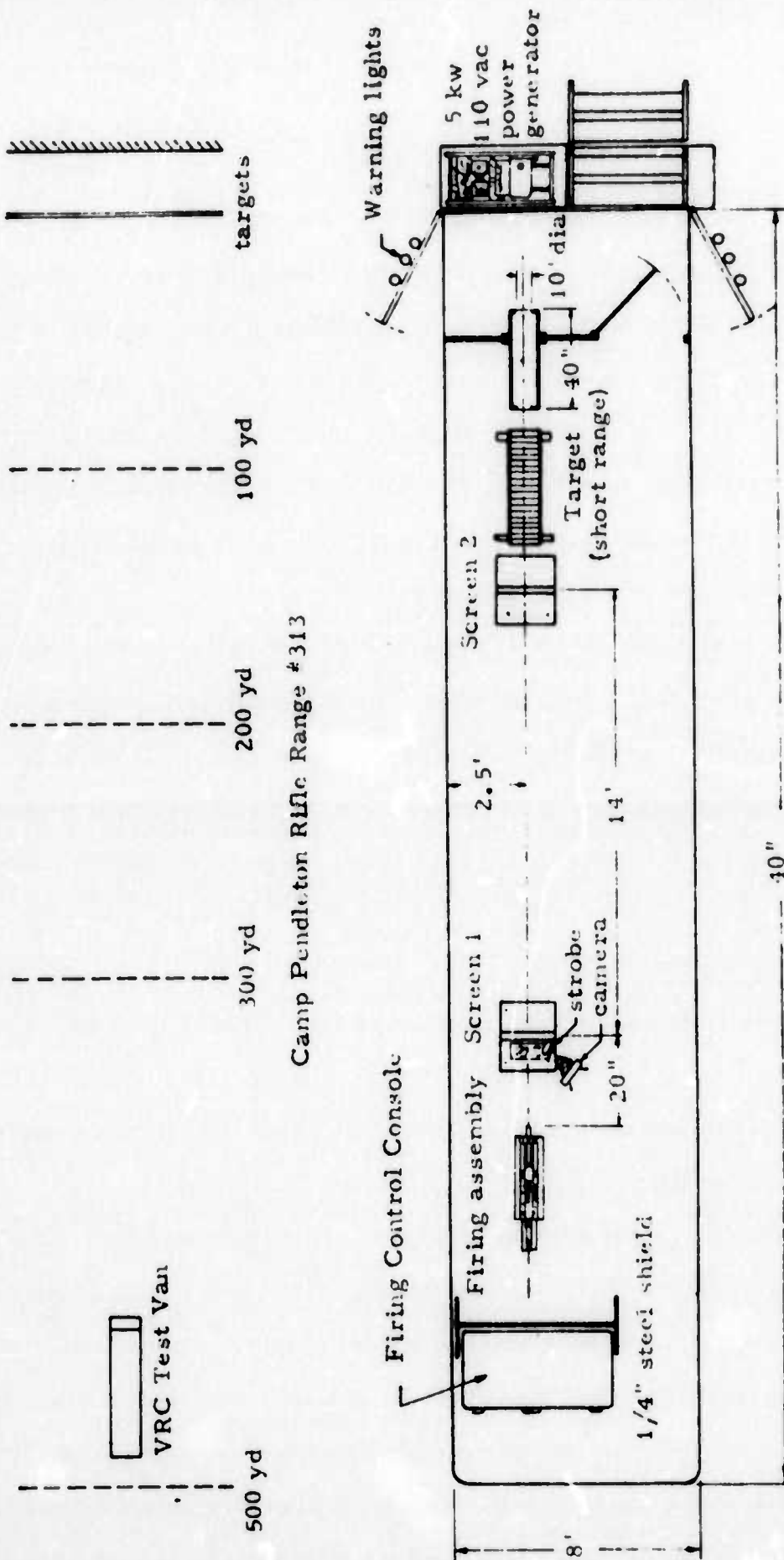
$$p = p_o \left[1 + \frac{\gamma-1}{2} M^2 \right]^{-\frac{\gamma}{\gamma-1}}$$

B. MOBILE FIRING RANGE TEST SETUP

1. Facility Description

A mobile test facility has been established by VRC at Camp Pendleton to conduct the firing tests of the hollow projectile. It consists of an instrumented storage van which serves as both a short firing range and a photographic dark room for obtaining pictures of the projectile in flight by means of stroboscopic flash photography. For long range firing the van doors are swung open, and the Camp Pendleton range facilities can be used without the necessity of moving and remounting the firing assembly. The overall test setup and interior test van arrangement are depicted in Fig. A-2.

The van is located near the 500 yard line as measured from the standard firing range targets. To obtain firing data as a function of



VRC Test Van General Arrangement

FIRING TEST SETUP

Fig. A-2

distance, a portable target is employed.

The interior arrangement of the test van has a ballistic screen (Electronic Counters, Inc., Model 6107) and chronograph (Electronic Counters, Inc., Model 4600) for measuring muzzle velocity. When the projectile passes through Screen 1, the pulse which triggers the chronograph is also used to trigger a strobe light (General Radio Model 1538) positioned to illuminate the projectile. The van is dark so the camera (Polaroid) shutter can be opened prior to firing. Thus, the projectile is photographed in flight.

A target consisting of stacked fiber boards is used for projectile recovery. For firing down range, this target is removed and the projectile is fired through a ten inch diameter hole cut in a light shielding box designed to minimize light entry in the "dark room" test van.

2. Test Procedures

The first step in the firing range test effort is to launch the projectile. This involves (1) achievement of the desired muzzle velocity, (2) separation of the projectile from the sabot and (3) impartation of spin for stability.

The launch velocity and energy for the given standard 7.62 mm test barrel (D755 3791) was analytically estimated as a function of projectile and sabot weight to propellant weight. Semi-empirical interior ballistic methods outlined in Ref. A-3 were employed. Suitable propellants were selected via established handloading methods.

The sabot and projectile must be designed to withstand the pressures ($\approx 50,000$ psi) and associated loads in the test barrel during

launching. This was first analytically investigated via stress analysis procedures outlined in Ref. A-4.

Then a systematic series of test firings (short range) were conducted to arrive at a reliable "workhorse" sabot configuration. As anticipated from stress and design calculations, detailed attention must be paid to manufacturing tolerances and handloading techniques. Failures of the sabot and/or projectiles in the test barrel were systematically eliminated via detailed redesigns during the process of arriving at a reliable workhorse system. Failures were detected photographically by the camera just downstream of the muzzle (Fig. A-2).

After the projectile is launched at the proper muzzle velocity, it is necessary to ensure that the projectile separates cleanly from the sabot while achieving the proper spin rate. Both of these factors were investigated and confirmed photographically. The character of the separation process could be directly viewed. The spin rate was indirectly ascertained by observing that the soft outer coating materials generally sheared-off if the full spin rate were not achieved. Additional verification of spin rate achievement was obtained by recovering projectiles and examining the rifling marks in the coating.

With achievement of clean sabot/projectile separations at the proper spin rate, the accuracy, dispersion and penetration characteristics of the projectile could be evaluated. To the extent possible, the test procedures were based on Ref. A-5. For example, the accuracy test data was reduced in terms of (1) mean radius, (2) extreme horizontal, (3) extreme vertical, and (4) extreme spread. These terms and the associated data reduction procedure are given in Ref. A-5.

APPENDIX REFERENCES

- A-1 Pope, Alan, and Goin, Kenneth L.: High Speed Wind Tunnel Testing, John Wiley and Sons, Inc., New York, 1965.
- A-2 Ames Research Staff: 'Equations, Tables, and Charts for Compressible Flow,' NACA Report 1135, Ames Aeronautical Laboratory, Moffett Field, California, 1953.
- A-3 U.S. Army Materiel Command: Interior Ballistics of Guns, Engineering Design Handbook, Ballistic Series, AMCP 706-150, February 1965.
- A-4 U.S. Army Materiel Command: Sabot Technology Engineering, Engineering Design Handbook, AMCP 706-445, July 1972.
- A-5 U.S. Army Materiel Command: Procurement Ammunition Ballistic Acceptance Methods, Volume 3, Test Procedures for 7.62 mm Cartridges, AMCR 715-505, February 1964.

Preceding page blank